A Tsunami Forecast Model for Cape Hatteras, North Carolina

Hongqiang Zhou[1,2] and NCTR

1. NOAA Center for Tsunami Research, Pacific Marine Environmental Laboratory, Seattle, WA
2. Joint Institute for the Study of the Atmosphere and Ocean, Seattle, WA

Contents

List of Figures

List of Tables

Abstract This report describes the development of a tsunami forecast model for Cape Hatteras, North Carolina. This model is to be incorporated into the Short-term Inundation Forcasting for Tsunamis (SIFT) system for the National Oceanic and Atmospheric Administration (NOAA). The forecast model includes a numerical model that simulates the nearshore wave propagation and coastal runup in three telescoped nested grids in real time. Cape Hatteras is covered by the innermost grid at a resolution of $3''$ ($\sim$ 93 m). The model is capable of completing a 12-hr simulation within approximately 22 min of CPU time on a 2×6 core @ 2.93 GHz workstation running in Linux 64 RH5 environment. Since there are no historical tsunami records for this area, the forecast model is tested using several synthetic scenarios of tsunamis generated in the Atlantic Basin. Computational results are compared between the present forecast model and a higher-resolution reference model. Results show very good agreement between the two models indicating reasonable accuracy of the forecast model. These tests also indicate that the forecast model has good stability under conditions of extremely high and low incoming waves.

1 Background and Objectives

The National Oceanic and Atmospheric Administration (NOAA) Center for Tsunami Research (NCTR) at the NOAA Pacific Marine Environmental Laboratory has developed a tsunami forecasting capability for operational use by NOAA's two Tsunami Warning Centers located in Hawaii and Alaska (Titov et al., 2005). The Short-term Inundation Forecasting for Tsunamis (SIFT) system is designed to provide quick and accurate basin-wide warning of approaching tsunami waves. This system combines real-time tsunami event data with numerical models to produce estimates of tsunami arrival times, wave amplitudes, and runup at coastal communities of interest. It integrates several key components: deep-ocean observations of tsunamis in real time, a basin-wide precomputed propagation database of water levels and flow velocities based on potential seismic unit sources, an inversion algorithm to refine the tsunami source based on deep-ocean observations during an event, and inundation forecast models run in real time and at high resolutions for selected coastal communities.

The SIFT system is planned to cover most of the tsunami-threatened U.S. communities, including Cape Hatteras, a populous recreational destination of North Carolina. Cape Hatteras is a bend of Hatteras Island, one of the long thin barrier islands that run roughly parallel to the continental coast, separating the Pamlico Sound from the Atlantic Ocean. Offshore of Cape Hatteras, the southerly cold water Labrador current collides with the northerly warm water Florida current, creating a large expanse of shallow sandbars, which extend more than 20 km into the ocean. The largest community of Cape Hatteras is Buxton, a town of 1,273 residents in 2010 (U.S. Census Bureau, 2010).

Cape Hatteras, like most U.S. communities along the Atlantic and Caribbean coasts, is susceptible to tsunamis generated in the Atlantic Basin. The most destructive tsunami in the Atlantic Basin was triggered by the 1755 Lisbon earthquake, which happened in the Azores-Gibraltar fault zone with a moment magnitude (Mw) of 8.5–9.0 (Gutscher et al., 2006). The tsunami ravaged the coasts of Southwest Iberia and Northwest Morocco, with maximum runups reaching 5–15 m (Baptista et al., 1998). The U.S. coasts were fortunately spared by this tsunami, mainly because of the specific source location, fault orientation, and the bathymetry in the Atlantic Ocean (Barkan et al., 2009). Besides earthquakes, potential submarine and subaerial landslides may also trigger tsunamis that threaten the U.S. Atlantic and Caribbean coasts (Driscoll et al., 2000; ten Brink et al., 2008).

In this study, we develop a tsunami forecast model for Cape Hatteras. This model is to be integrated into the SIFT system as a part of NOAA's effort to provide a nation-wide tsunami forecast capability.

2 Forecast Methodology

A forecast model computes tsunami arrival times, wave heights, and runup in a specific coastal community in real time during a tsunami event. In the SIFT system, all the models are designed and tested to perform under stringent time constraints, given that time is generally the single limiting factor in saving lives and properties. Computations in a forecast model are performed with a numerical code, Method of Splitting Tsunami (MOST), which solves the characteristic formulation of the shallow water equations through a finite difference scheme. This code has been extensively validated against laboratory experiments and

analytical benchmarks (Synolakis et al., 2008).

Basin-scale computations of tsunami propagation can be very time-consuming and is almost impossible in real-time forecast at present. Instead of real-time simulation, propagation of water waves in the ocean basins due to a "unit earthquake source" is precomputed and the time series of water surface elevations and water velocities are stored in the propagation database as a "unit tsunami source function". A unit earthquake source has a measurement of 100×50 km^2 in area and a slip value of 1 m, equivalent to the moment magnitude (Mw) of 7.5 (Gica et al., 2008). All subduction zones in the ocean basins are split into numerous unit earthquake sources. Given that the tsunami evolution in deep ocean is a linear process (Kânoğlu and Synolakis, 2006), a tsunami scenario can be accurately represented through the linear combination of related source functions. During a tsunami event, as the waves propagate across the ocean and successively reach the Deep-Ocean Assessment and Reporting of Tsunamis (DART) observation sites, measured water surface displacements are ingested into the tsunami forecast application in near real time and incorporated into an inversion algorithm to produce an improved estimate of the tsunami source (Percival et al., 2011).

Nonlinear effects become significant when the waves enter the nearshore shallower water. This process is simulated in real time in the tsunami forecast model. The forecast model includes three telescoped, nested grids, named A, B, and C grids, at successively increased resolutions. The outermost A grid provides a smooth transition from the propagation database to the nearshore real-time simulation. The A grid covers a large domain with offshore boundaries extended into deep ocean. During a tsunami event, synthetic boundary conditions are obtained along the open boundaries of this grid through the linear combination of tsunami source functions. The population and economic center of the target community is covered by the C grid at a high resolution in order to represent the details of bathymetry and topography, as well as to mitigate numerical errors in the numerical model. All these grids are constructed based on the digital elevation models (DEMs) developed by the National Geophysical Data Center (NGDC) and NCTR. Technical aspects of forecast model development, validation and stability testing have been reported by Titov and González (1997). Details of forecast methodology can be found in the publication of Tang et al. (2009). The accuracy and efficiency of tsunami forecast models in the Pacific region currently implemented in the SIFT system have been validated in recent tsunami events (Titov et al., 2005; Titov, 2009; Tang et al., 2008; Wei et al., 2008).

3 Model Development

The accuracy of tsunami forecast largely relies on the accuracy of bathymetric and topographic data employed in the computational grids. The grids in the Cape Hatteras forecast model are developed based on the DEMs provided by NGDC, and we consider it to be an adequate representation of the local topography and bathymetry. As new DEMs become available, forecast models will be updated and report updates will be posted at "`http://nctr.pmel.noaa.gov/forecast_reports`".

From these DEMs, a "reference" model is first developed. This model has very high resolutions in the three grids and simulates the wave processes without observable numerical errors. Due to the high resolutions, the reference model consumes very long CPU times

and should not be applied to real-time forecast. By downgrading the resolutions, and sometimes reducing the domain coverage, of the reference model grids, an "optimized" model is developed. The objective of this optimization is to limit the CPU time below an operationally specific period, ideally 10 min for a 4-hr simulation. This model is referred to as the "optimized tsunami forecast model", or simply the "forecast model".

3.1 The DEMs

NGDC has developed a 1/3 arc sec DEM of Cape Hatteras (Taylor et al., 2006), which covers an area between 34.75°N and 35.8°N latitude and 76.05°W and 75.05°W longitude. The DEM is referenced to the World Geodetic System (WGS84) horizontal datum and Mean High Water (MHW). The high-resolution bathymetric and topographic data were obtained from numerous sources, which include

1. the "Global Shoreline Data" digital shoreline from the National Geospatial-Intelligence Agency;
2. 46 hydrographic surveys by NOAA National Ocean Services;
3. three electronic nautical charts from NOAA Office of Coast Survey;
4. deep-water multibeam surveys of the U.S. Atlantic margin conducted by University of New Hampshire's Center for Coastal and Ocean Mapping/Joint Hydrographic Center;
5. the 5-m topographic LiDAR data collected and processed by the North Carolina Division of Emergency Management, Floodplain Mapping Program; and
6. the high-resolution combined topographic/bathymetric LiDAR surveys of the North Carolina open-ocean coastline conducted by the Joint Airborne Lidar Bathymetry Technical Center of Expertise.

A 9 arc sec DEM was developed by NGDC to cover the U.S. Atlantic coast (NGDC, 2005). This DEM covers an area from 25°N to 50°N latitude and 85°W to 50°W longitude. It is referenced to the WGS84 horizontal datum. Unlike the 1/3 arc sec DEM, no conversion to a common vertical datum was performed for this grid. The data sources from which this DEM was compiled include

1. the NOAA Medium Resolution Digital Vector Shoreline compiled from NOAA coastal charts by the Strategic Environmental Assessments Division of NOAA's Office of Ocean Resources Conservation and Assessment;
2. multibeam surveys from NOS and NOAA Ocean Exploration, Scripps Institute of Oceanography, University of Rhode Island, Woods Hole Oceanographic Institution, Lamont-Doherty Earth Observatory, and U.S. Geological Survey;
3. hydrographic survey data from the NOS Hydrographic Surveys Database; and
4. unpublished bathymetric LiDAR data collected by the Joint Airborne LiDAR Bathymetry Technical Center of Expertise and provided by the U.S. Army Corps of Engineers;

3.2 Forecast area

Figure 1 shows a satellite image of Cape Hatteras obtained from Google Maps. The semi-closed water body of Pomlico Sound is well protected by Hatteras Island from potentially devastating water waves that may be generated by tsunamis or hurricanes in the Atlantic Ocean. The location of Hatteras Island's major community, Buxton, on the inner side of the island suggests that it is less vulnerable to potential tsunami hazards compared with other small Atlantic shore towns, such as Frisco. NOAA operates a tide station on the Cape Hatteras Fishing Pier (35°13.4′N, 75°38.1′W). This station was established on 24 May 1973 and has been in its present installation since 16 June 1994. The mean tide range at this station is 0.91 m. Maximum water level is 0.84 m above Mean Higher High Water (MHHW) and minimum water level is 0.70 m below MHHW.

3.3 Grid setup

The continental shelf offshore of the U.S. Atlantic coast extends nearly 100 km into the ocean. Water depth over the continental shelf is mostly less than 50 m. When the long waves propagate from deep ocean into shallow water, nonlinear effects become stronger in the wave shoaling processes. These processes are computed in the A grid of the reference model (Figure 2a) at a resolution of 12 arc sec. Boundary conditions of this grid are derived from the propagation database. The B grid (Figure 2b) is nested immediately to the A grid and employs its computational results as the prescribed boundary conditions. The resolution in this grid is 6 arc sec. Simulations in the C grid (Figure 2c), which covers Cape Hatteras at a resolution of 1 arc sec, are performed with boundary conditions derived from the numerical results in B grid. Compared with the reference model, the forecast model has the same geographic coverage in the A grid (Figure 3a) but a lower resolution (24 arc sec). The B and C grids in the forecast model (Figures 3b and 3c) cover smaller areas than those of the reference model. Resolutions are 8 and 3 arc sec in the B and C grids, respectively. The configuration parameters of these grids are listed in Table 1. Input parameters for the numerical models are presented in Appendix A.

In both the reference and forecast models, time series of simulated water surface elevations are output at a warning point in the C grids. The warning point is a grid node that is the nearest to the location of the tide station. During a tsunami event, the time series output from the forecast model at the warning point can be compared with those measured by the tide gauge to evaluate the accuracy of the forecast. The actual location of warning point in the forecast model is (35.2228°N, 75.6352°W), where the water depth is 4.51 m. In the reference model, the warning point is at (35.2227°N, 75.6352°W) and the water depth is 4.77 m at this site.

4 Model Testing

A forecast model needs to be tested for accuracy and stability before it is integrated into the SIFT system and deployed for operations. Due to the lack of past tsunami records in the Cape Hatteras area, the present model is tested in several synthetic scenarios.

4.1 Accuracy

Computational results of a numerical model can be affected by the bathymetric and topographic errors in the grids. The development of the forecast model for Cape Hatteras employs the best available datasets of bathymetry and topography to minimize these errors. Grid resolution is another factor affecting the accuracy of a numerical model. Lower resolution can introduce more errors. Because of the second-order finite difference scheme employed by MOST, the magnitude of numerical errors is a square function of the spacing of grid nodes. If the resolution is sufficiently high, further increasing or decreasing resolution may not affect the numerical accuracy significantly. Because of the very high resolutions in its grids, numerical errors are negligible in the reference model. The forecast model grids are developed from the reference grids by downgrading their resolutions. By comparing the numerical results in the same scenarios between the two models, we investigate if considerable numerical errors are introduced in the forecast model during this process.

The synthetic scenarios include six mega tsunamis due to Mw 9.1 earthquakes, a tsunami generated by a Mw 7.5 earthquake, and a micro tsunami caused by a Mw 6.2 earthquake. Unit sources involved in these scenarios are listed in Table 2, and earthquake epicenters for the six mega tsunamis are plotted in Figure 4. Parameters of unit sources in the Atlantic Basin currently developed in the SIFT system can be found in Appendix B. All scenarios, except the micro tsunami, are simulated with both reference and forecast models. Figures 5–11 present the numerical results. In scenario ATSZ 48-57 (Figure 6), the two models predict slightly different inundation extents near the coast of Pomlico Sound. This shows the effect of different model resolutions and grid extents. In general, we note very good agreement between the two models in the maximum water surface elevations and speeds near Cape Hatteras. At the warning points, minor differences in the time series of water levels are present in the trailing waves of relatively shorter wavelengths. For the purpose of operational forecast, we believe the accuracy of the forecast model is sufficient.

Though all mega tsunami scenarios have the same earthquake magnitude, their impacts on the Cape Hatteras area are very different. The highest wave heights and most severe coastal inundation are observed in scenario ATSZ 48-57, which is due to an earthquake along the northeast edge of the Caribbean Plate. After generated, water waves propagate from the source region towards Cape Hatteras without significant interference with islands in their passage. In this scenario, most of the dry land in Cape Hatteras is flooded. In contrary, in scenario ATSZ 68-77, most of the wave energy is blocked by the Greater Antilles and may not cause considerable impact on Cape Hatteras and other coastal communities outside the Caribbean region.

4.2 Stability

Stability is as important as accuracy in determining the reliability of a tsunami forecast model. When the incoming waves are very high, the rapidly moving shorelines and extremely steep wavefronts may cause the instability of the numerical model. The six mega tsunami scenarios represent events of extremely high waves, which are historically very rare in the Atlantic Ocean. Among these scenarios, ATSZ 48-57 induces the highest wave heights in the Cape Hatteras area. As shown in Figure 12, no stability issue is observed in this simulation.

The forecast model may also become instable when the incoming waves are extremely low. In this situation, the magnitude of numerical errors may become larger than those of the water waves and current speeds, and accumulate quickly causing computer memory overflow. A micro tsunami scenario, SSSZ B11, is employed to investigate the performance of the forecast model under this condition. Because the earthquake is very weak and far from the Cape Hatteras area, incoming wave heights are too low along the boundaries of the A grid to trigger the real-time simulation in the forecast model, which has a threshold of 0.001 m of input wave amplitudes. This threshold is temporarily lowered to 1.0×10^{-5} m in this test. Figure 13 plots the maximum water surface elevations in the three forecast grids. Despite the considerable build up of numerical errors during the 12-hr simulation, the forecast model has not crashed. Note that when this model is integrated into the SIFT system, the threshold of incoming wave amplitudes will be set to 0.001 m, and such an extremely weak event will not trigger the computation in the forecast model.

5 Conclusions

In this report, we develop a tsunami forecast model for Cape Hatteras, which is to be integrated into the SIFT system as an effort to provide forecast of tsunami arrival times, wave heights, and coastal runups for U.S. communities with potential tsunami threats. The forecast model includes a numerical model, which simulates the tsunami propagation and inundation in three levels of nested grids. Cape Hatteras is covered by the innermost grid at a resolution of 3 arc sec ($\sim$ 93 m). The model is capable of completing a 12-hr simulation in less than 30 min of CPU time as tested on a 2×6 core @ 2.93 GHz computer operating in linux 64 RH4 environment.

Due to the lack of historical tsunami data in this area, the forecast model is tested in several synthetic scenarios. Numerical accuracy of the forecast model is evaluated by comparing its computational results with those of a higher-resolution reference model. Good agreement between the two models indicates that the forecast model has reasonably good accuracy. The performance of the forecast model in the synthetic mega and micro tsunami scenarios also suggests that it is expected to work stably in real-time operations.

We further note that a potential megathrust earthquake along the northeast edge of the Caribbean Plate may cause severe tsunami impact on the Cape Hatteras area. In such an event, nearshore wave heights may exceed 8 m and most of the dry land may be flooded.

The Cape Hatteras tsunami forecast model has been incorporated into the SIFT system. Appendix C presents a test of this model with SIFT 3.2 for three synthetic scenarios. The test shows very good consistence between the results in this report and from the SIFT system. Good stability of this model is also observed in the test.

Acknowledgments

The work of model development described in this report was initiated by A. Mercado. This study is funded by the Joint Institute for the Study of the Atmosphere and Ocean (JISAO) under NOAA Cooperative Agreement Numbers NA10OAR4320148 and NA08OAR4320899, and is JISAO contribution number No. 2428. This work is also Contribution No. 3365 from NOAA/Pacific Marine Environmental Laboratory.

References

Baptista, M.A., Heitor, S., Miranda, J.M., Miranda, P.M.A., and Mendes Victor, L. (1998). The 1755 Lisbon; evaluation of the tsunami parameters, *J. Geodyn.*, *25*, 143–157.

Barkan, R., ten Brink, U.S., and Lin, J. (2009). Far field tsunami simulations of the 1755 Lisbon earthquake: Implications for tsunami hazard to the U.S. East Coast and the Caribbean, *Marine Geology*, *264*, 109–122.

Driscoll, N. W., Weissel, J. K., and Goff, J. A. (2000). Potential for large-scale submarine slope failure and tsunami generation along the U.S. mid-Atlantic coast, *Geology*, *20*(5), 4407–4410.

Gica, E., Spillane, M. C., Titov, V. V., Chamberlin, C. D., and Newman, J. C. (2008). Development of the forecast propagation database for NOAAs Short-Term Inundation Forecast for Tsunamis (SIFT), *NOAA Tech. Memo. OAR PMEL-139*, Pacific Marine Environmental Laboratory, NOAA, Seattle, WA, 89 pp.

Gutscher, M.-A., Baptista, M.A., and Miranda, J.M. (2006). The Gibraltar Arc Seismogenic zone: Part 2. Constraints on a shallow east dipping fault plane source for the 1755 Lisbon earthquake provided by tsunami modeling and seismic intensity. *Tectonophysics*, *426*, 153–166.

Kânoğlu, U., and Synolakis, C.E. (2006). Initial value problem solution of nonlinear shallow water wave equations, *Phys. Rev. Lett.*, *97*(14), 148501, doi:10.1103/PhysRevLett.97.148501.

National Geophysical Data Center (2005). East coast and Gulf coast and Caribbean nine second tsunami propagation grids compilation report, Prepared for the NOAA Center for Tsunami Inundation Mapping Efforts by the National Geophysical Data Center, 11pp.

Percival, D. B., Denbo, D. W., Eble, M. C., Gica, E., Mofjeld, H. O., Spillane, M. C., Tang, L., and Titov, V. V. (2011). Extraction of tsunami source coefficients via inversion of DART®buoy data, *Nat. Hazards*, *58*(1), doi: 10.1007/s11069-010-9688-1, 567–590.

Synolakis, C. E., Bernard, E. N., Titov, V. V., Kânoğlu, U., and González, F. I. (2008). Validation and verification of tsunami numerical models, *Pure Appli. Geophys.*, 165(11-12), 2197–2228.

Tang, L., Titov, V. V., Wei, Y., Mofjeld, H. O., Spillane, M., Arcas, D., Bernard, E. N., Chamberlin, C. D., Gica, E., and Newman, J. (2008). Tsunami forecast analysis for the May 2006 Tonga tsunami, *J. Geophys. Res.*, *113*, C12015, doi: 10.1029/2008JC004922.

Tang L., Titov, V. V., and Chamberlin, C. D. (2009). Development, testing, and applications of site-specific tsunami inundation models for real-time forecasting, *J. Geophys. Res.*, *6*, doi: 10.1029/2009JC005476.

ten Brink, U., Twichell, D., Geist, E., Chaytor, J., Locat, J., Lee, H., Buczkowski, B., Barkan, R., Solow, A., Andrews, B., Parsons, T., Lynett, P., Lin, J., and Sansoucy, M. (2008). Evaluation of tsunami sources with the potential to impact the U.S. Atlantic and Gulf coasts, USGS Administrative Report to the Nuclear Regulatory Commission, 300 pp.

Taylor, L.A., Eakins, B.W., Carignan, K.S., Warnken, R.R., Schoolcraft, D.C., and Sharman, G.F. (2006). Digital elevation model for Cape Hateras, North Carolina: Procedures, data sources and analysis. National Geophysical Data Center, NOAA, Boulder, Colorado, 18 pp.

Titov, V. V. and González, F. I. (1997). Implementation and testing of the Method of Splitting Tsunami (MOST) model, *NOAA Tech. Memo*, *ERL PMEL-112*, Pacific Marine Environmental Laboratory, NOAA, Seattle, WA, 11 pp.

Titov V. V., González F. I., Bernard E. N., Eble M. C., Mofjeld H. O., Newman J. C., Venturato A. J. (2005). Real-time tsunami forecasting: challenges and solutions, *Nat. Hazards*, 35, 41–58.

Titov, V. V. (2009). Tsunami forecasting. In: E. N. Bernard and A. R. Robinson (edited) *The Sea*, Vol. 15, Chapter 12, Harvard University Press, Cambridge, MA, and London, U.K., 371–400.

U.S. Census Bureau (2010). American FactFinder Fact Sheet: Buxton CDP, North Carolina, retieved April 23, 2014, from: `http://factfinder2.census.gov/faces/tableservices/jsf/pages/productview.xhtml?src=bkmk`.

Wei, Y., Bernard, E. N., Tang, L., Weiss, R., Titov, V. V., Moore, C., Spillane, M., Hopkins, M., and Kânoğlu, U. (2008). Real-time experimental forecast of the Peruvian tsunami of August 2007 for U.S. coastlines, *Geophys. Res. Lett.*, *35*, L04609, doi:10.1029/2007GL032250.

Figures

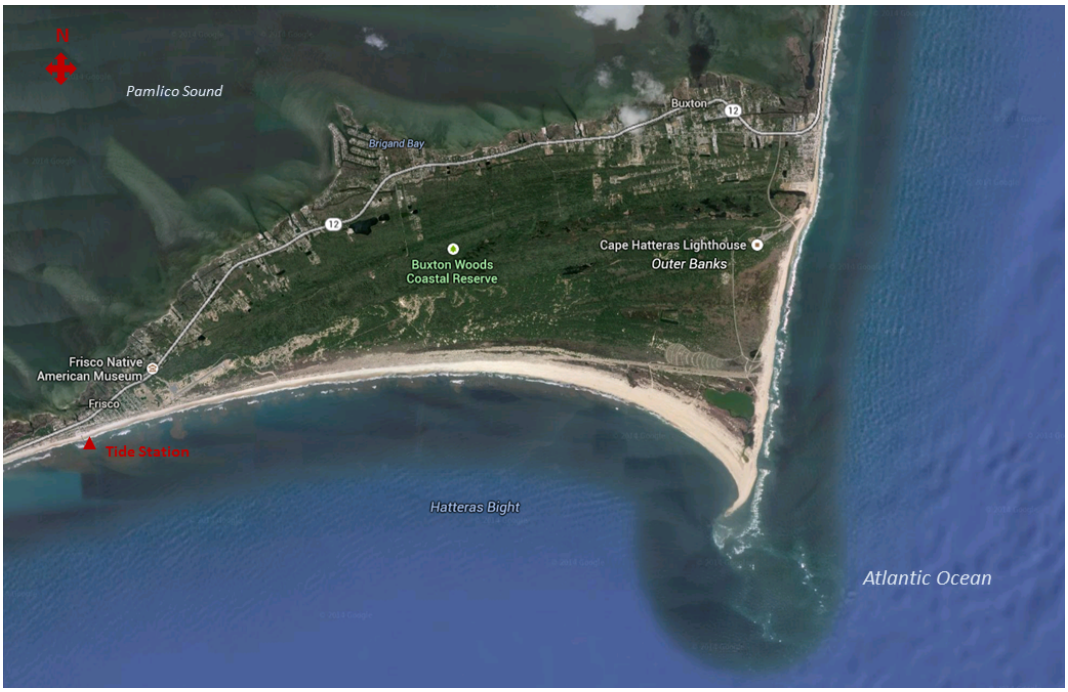

Figure 1: A satellite image of Cape Hatteras, North Carolina (courtesy of "Google Maps").

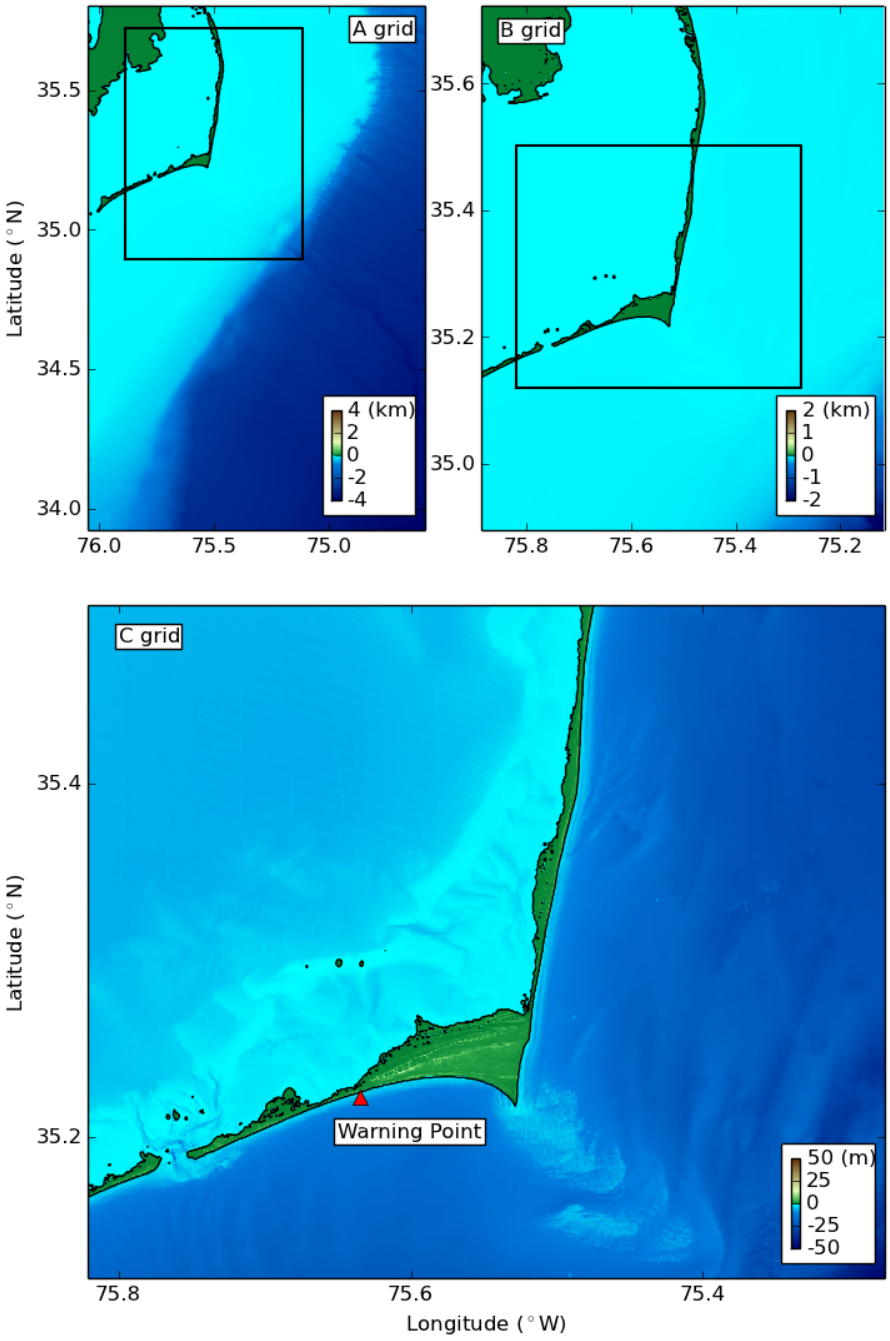

Figure 2: Computational grids of the reference model for Cape Hatteras, North Carolina.

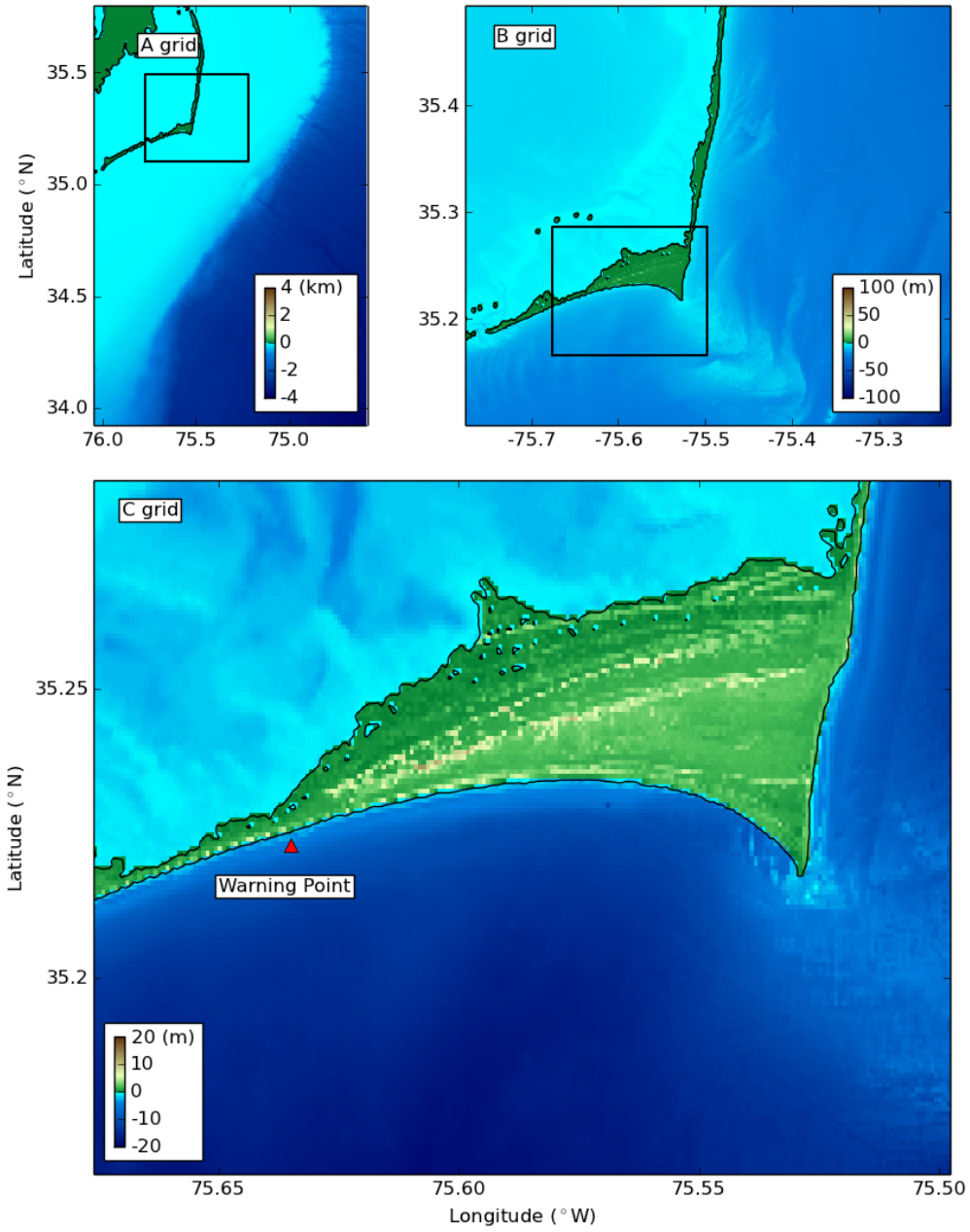

Figure 3: Computational grids of the forecast model for Cape Hatteras, North Carolina.

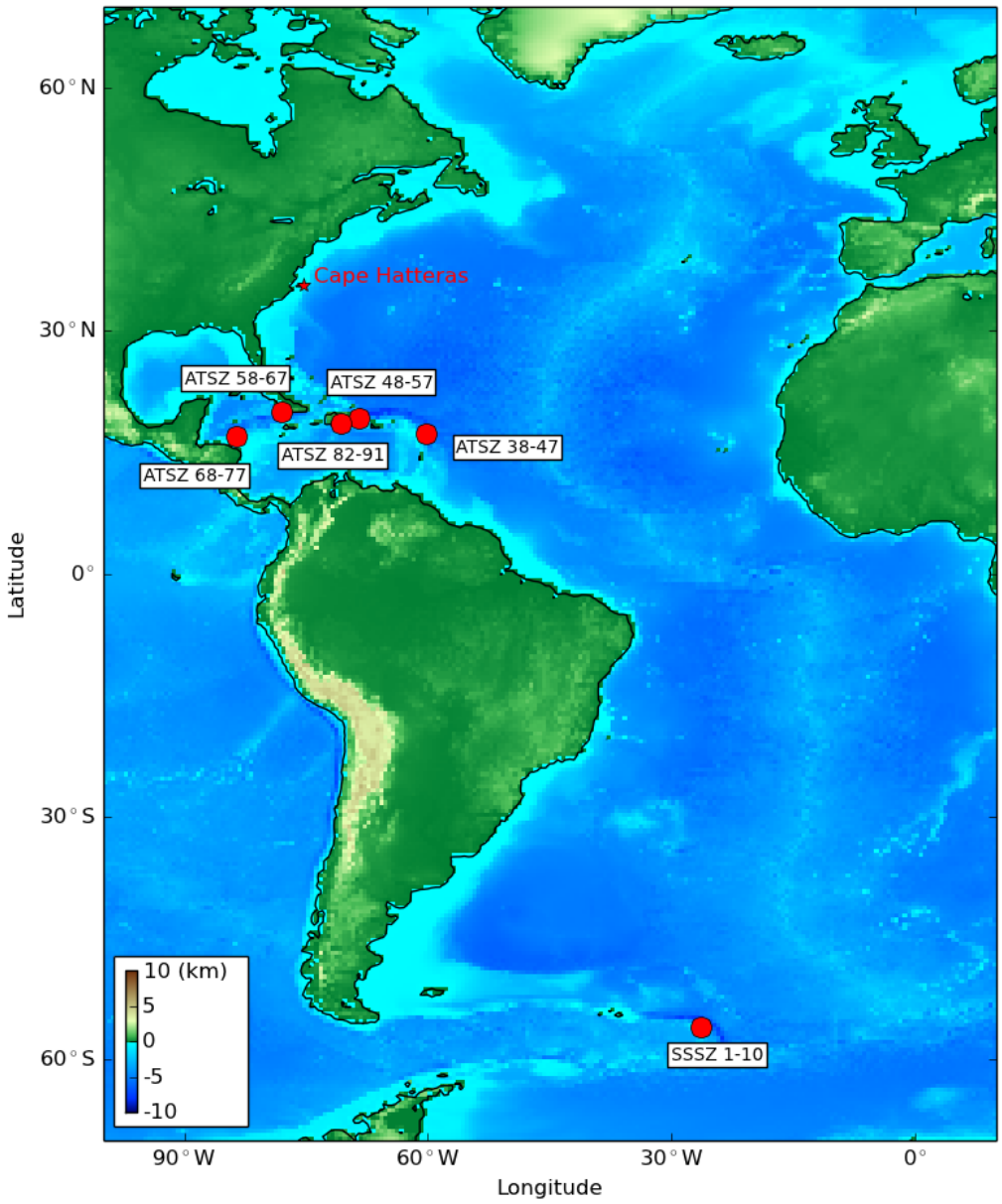

Figure 4: Epicenters of triggering earthquakes in synthetic mega tsunami scenarios employed to test the Cape Hatteras, North Carolina, forecast and reference models.

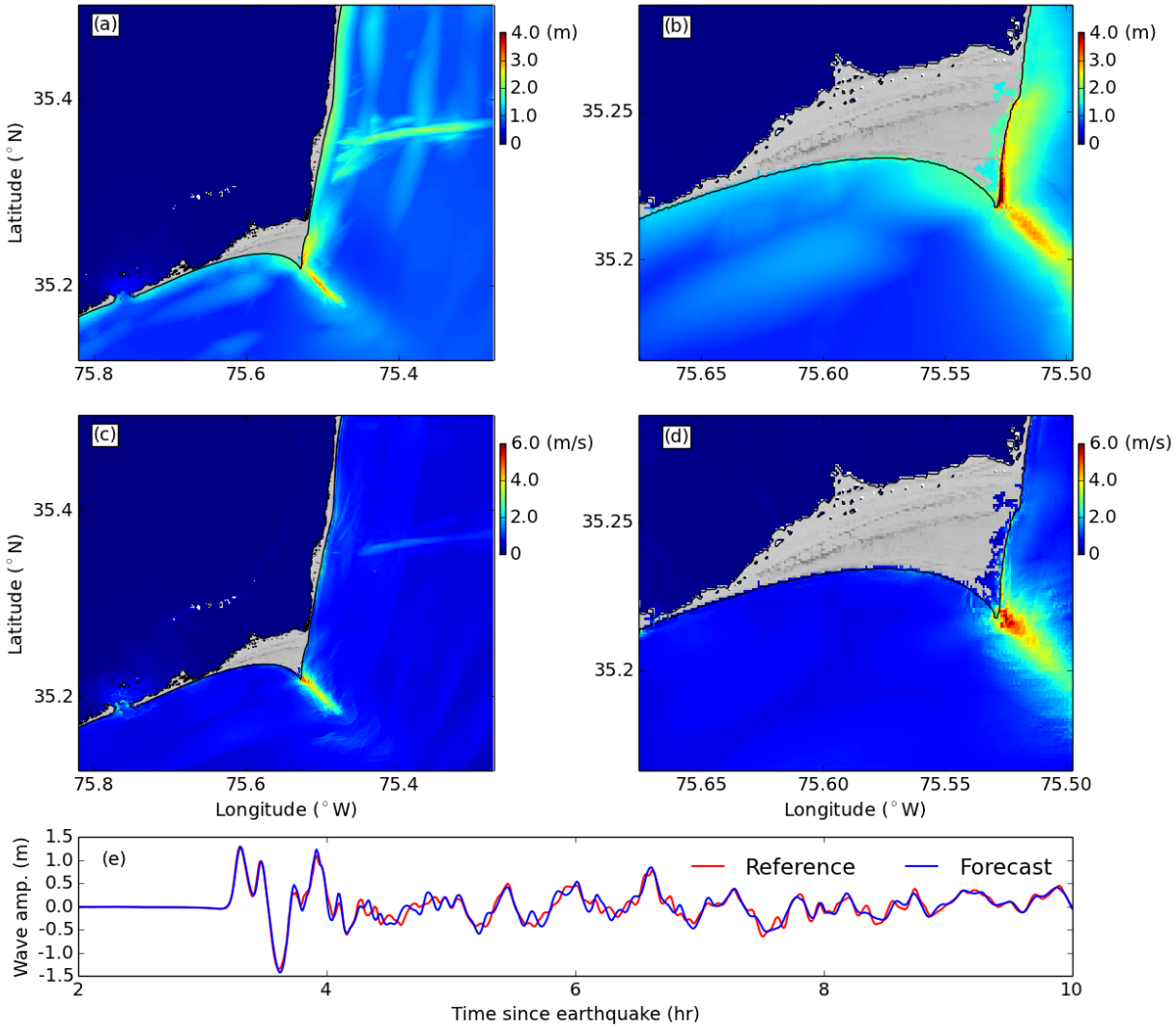

Figure 5: Numerical results for the synthetic scenario of ATSZ 38-47: maximum water surface elevations near Cape Hatteras, North Carolina, predicted by the reference (a) and forecast models (b), maximum water speeds near Cape Hatteras predicted by the reference (c) and forecast models (d), and time series of wave amplitudes at the warning point (e).

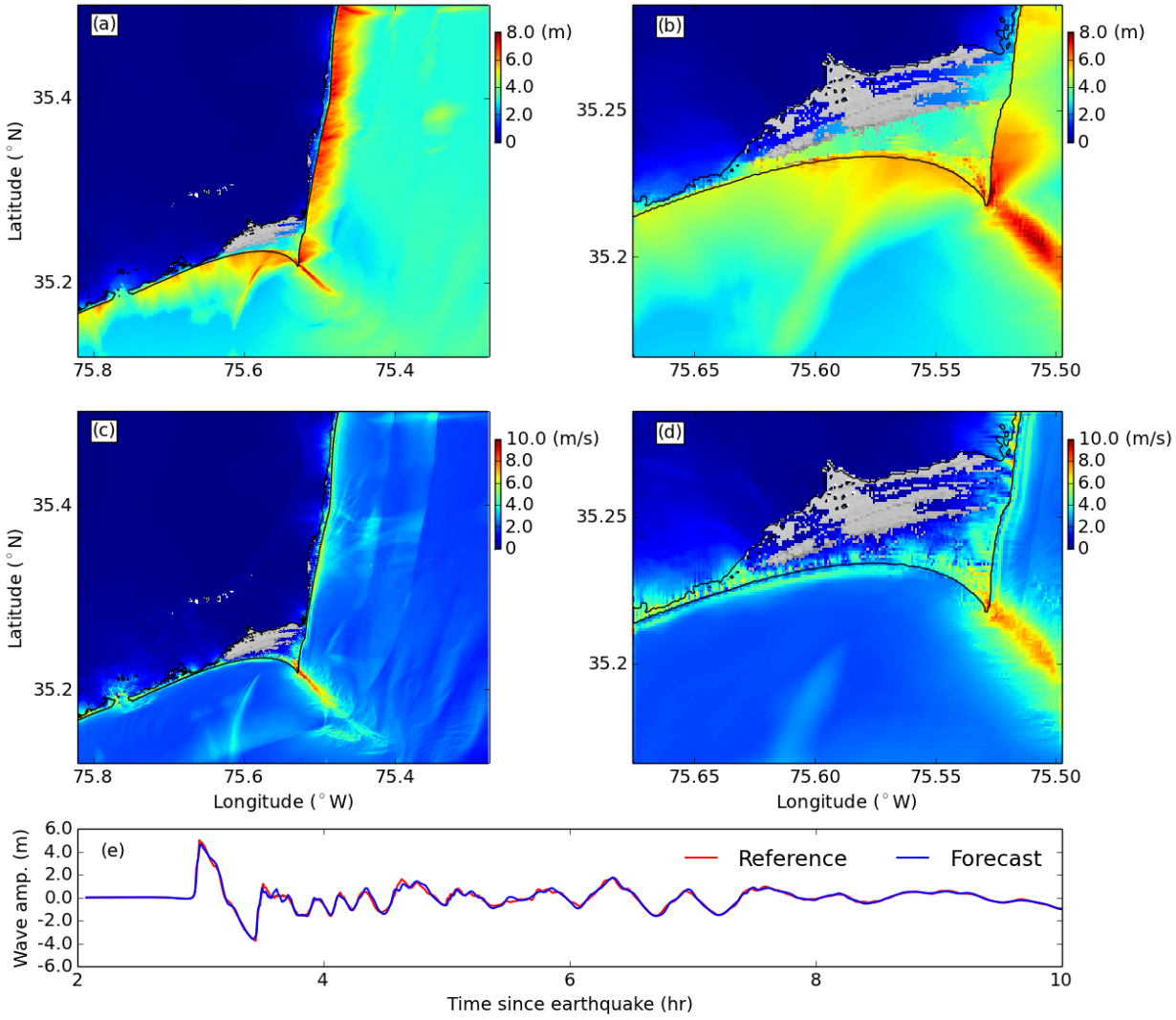

Figure 6: Numerical results for the synthetic scenario of ATSZ 48-57: maximum water surface elevations near Cape Hatteras, North Carolina, predicted by the reference (a) and forecast models (b), maximum water speeds near Cape Hatteras predicted by the reference (c) and forecast models (d), and time series of wave amplitudes at the warning point (e).

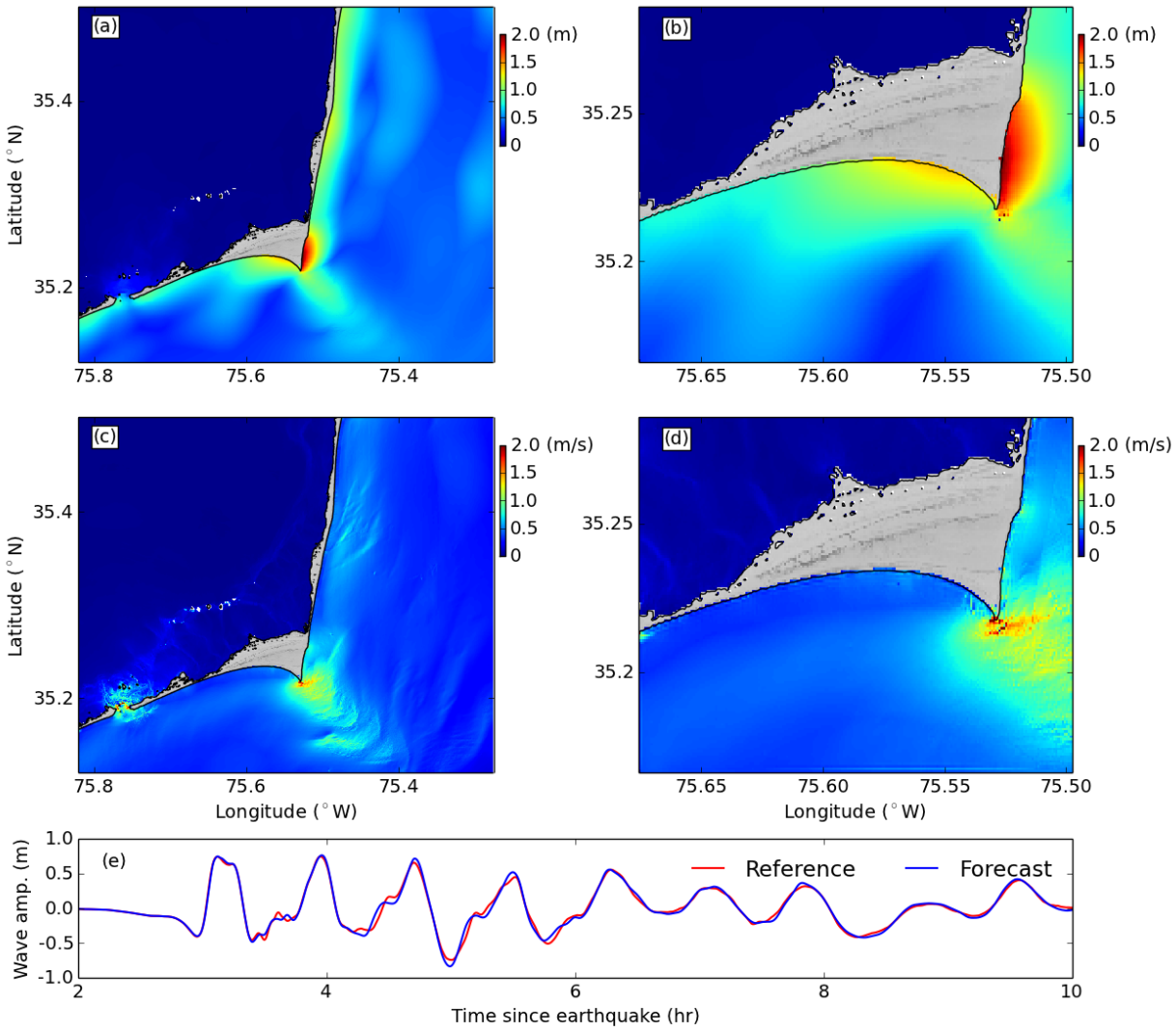

Figure 7: Numerical results for the synthetic scenario of ATSZ 58-67: maximum water surface elevations near Cape Hatteras, North Carolina, predicted by the reference (a) and forecast models (b), maximum water speeds near Cape Hatteras predicted by the reference (c) and forecast models (d), and time series of wave amplitudes at the warning point (e).

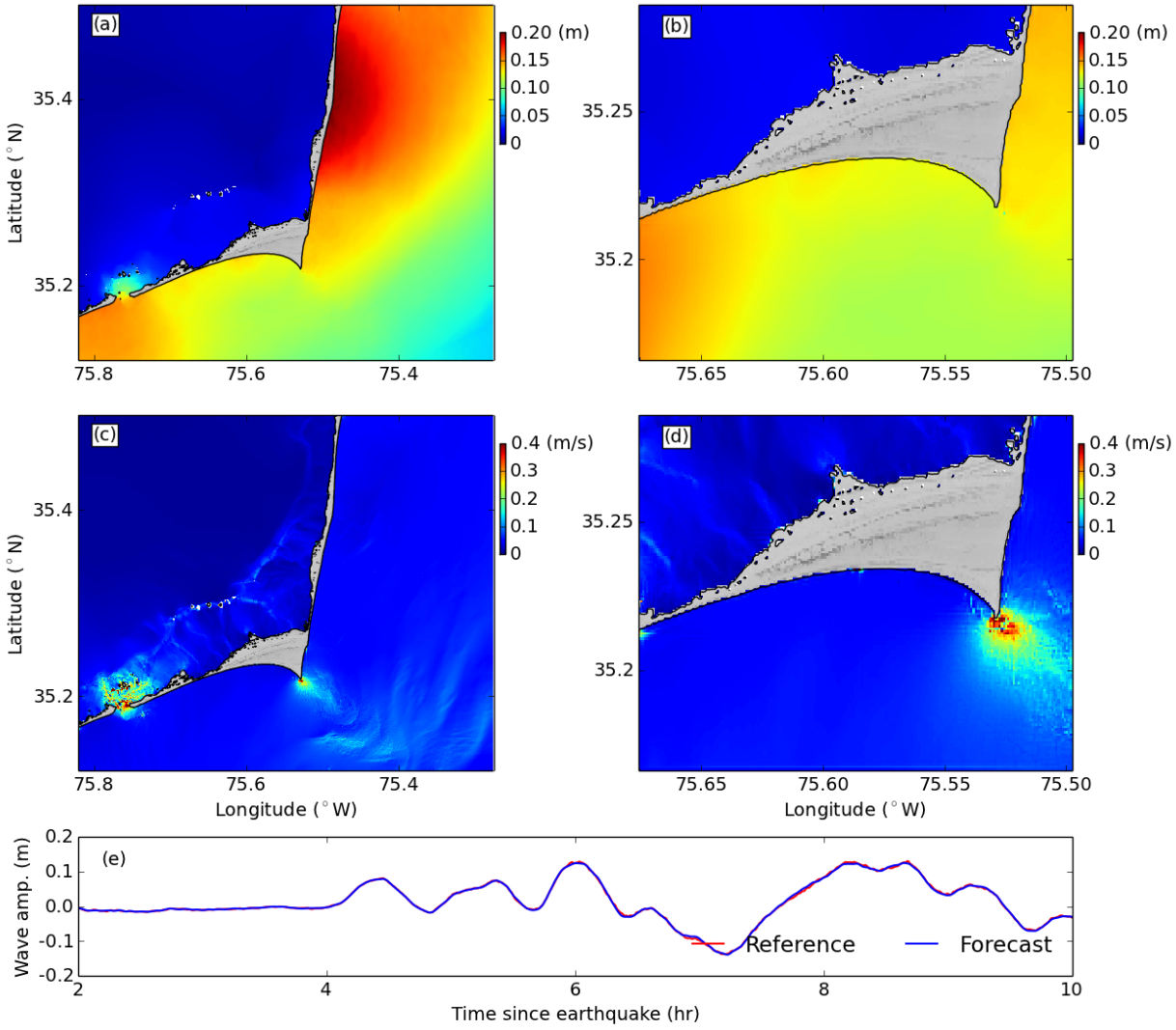

Figure 8: Numerical results for the synthetic scenario of ATSZ 68-77: maximum water surface elevations near Cape Hatteras, North Carolina, predicted by the reference (a) and forecast models (b), maximum water speeds near Cape Hatteras predicted by the reference (c) and forecast models (d), and time series of wave amplitudes at the warning point (e).

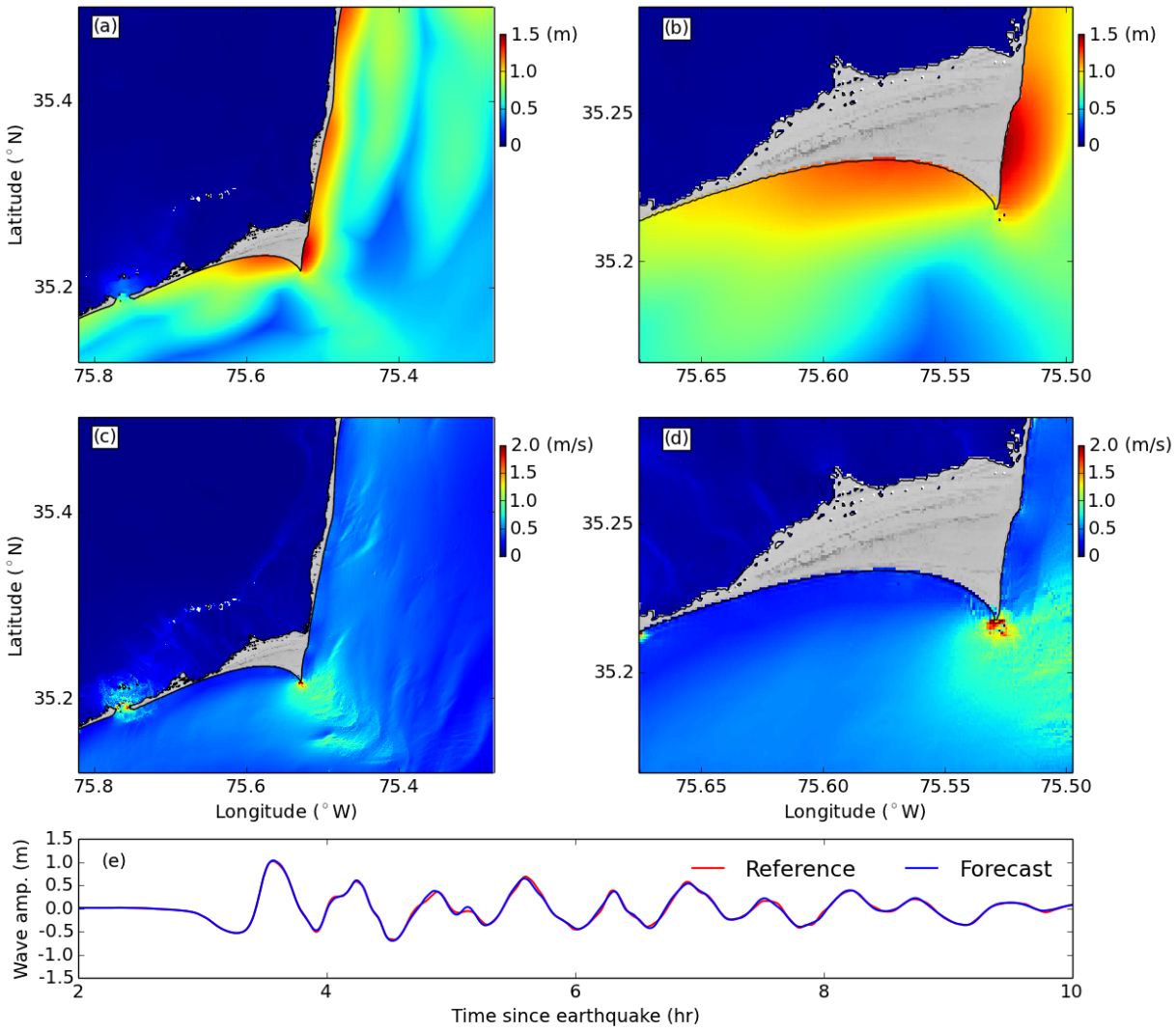

Figure 9: Numerical results for the synthetic scenario of ATSZ 82-91: maximum water surface elevations near Cape Hatteras, North Carolina, predicted by the reference (a) and forecast models (b), maximum water speeds near Cape Hatteras predicted by the reference (c) and forecast models (d), and time series of wave amplitudes at the warning point (e).

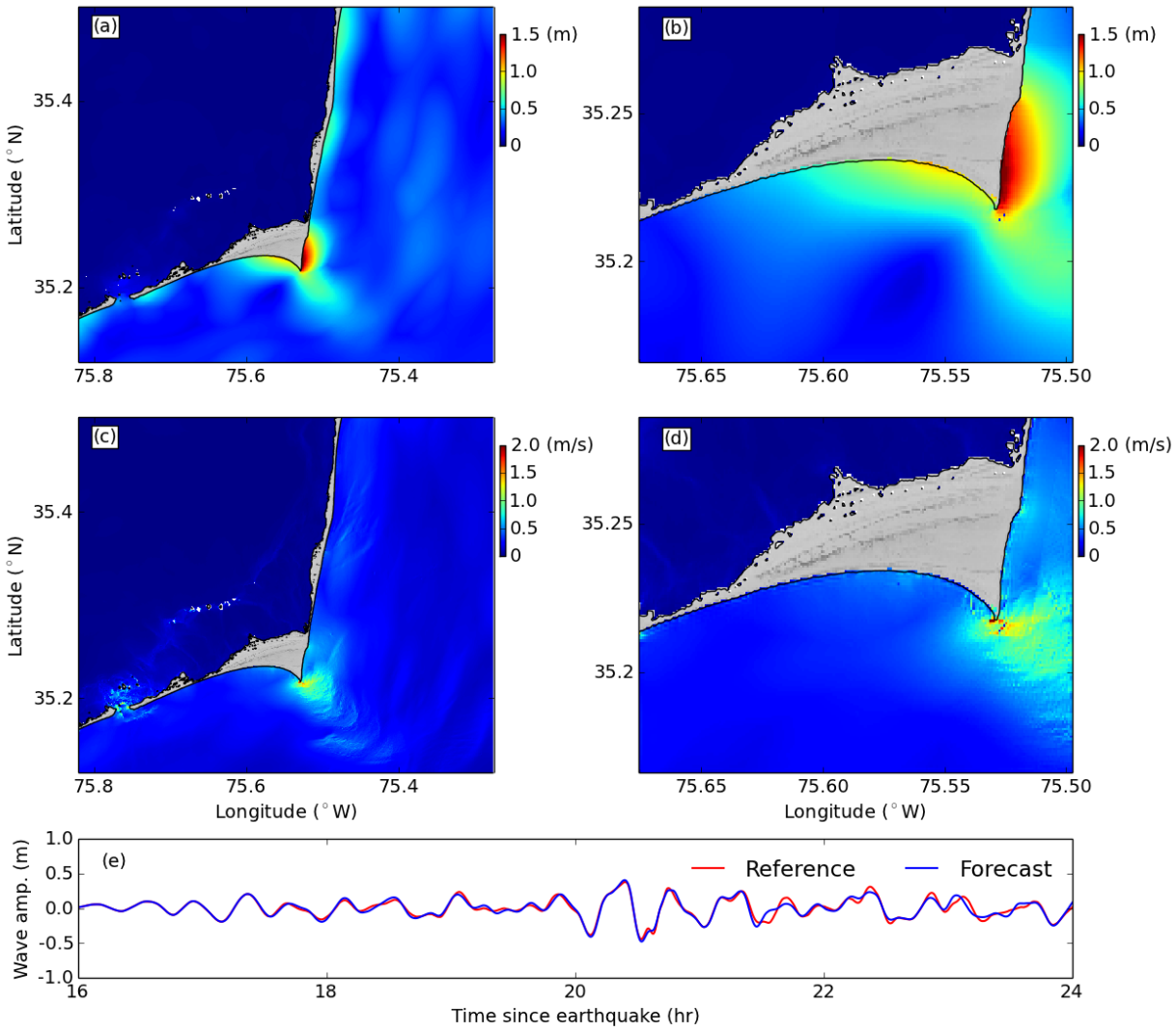

Figure 10: Numerical results for the synthetic scenario of SSSZ 1-10: maximum water surface elevations near Cape Hatteras, North Carolina, predicted by the reference (a) and forecast models (b), maximum water speeds near Cape Hatteras predicted by the reference (c) and forecast models (d), and time series of wave amplitudes at the warning point (e).

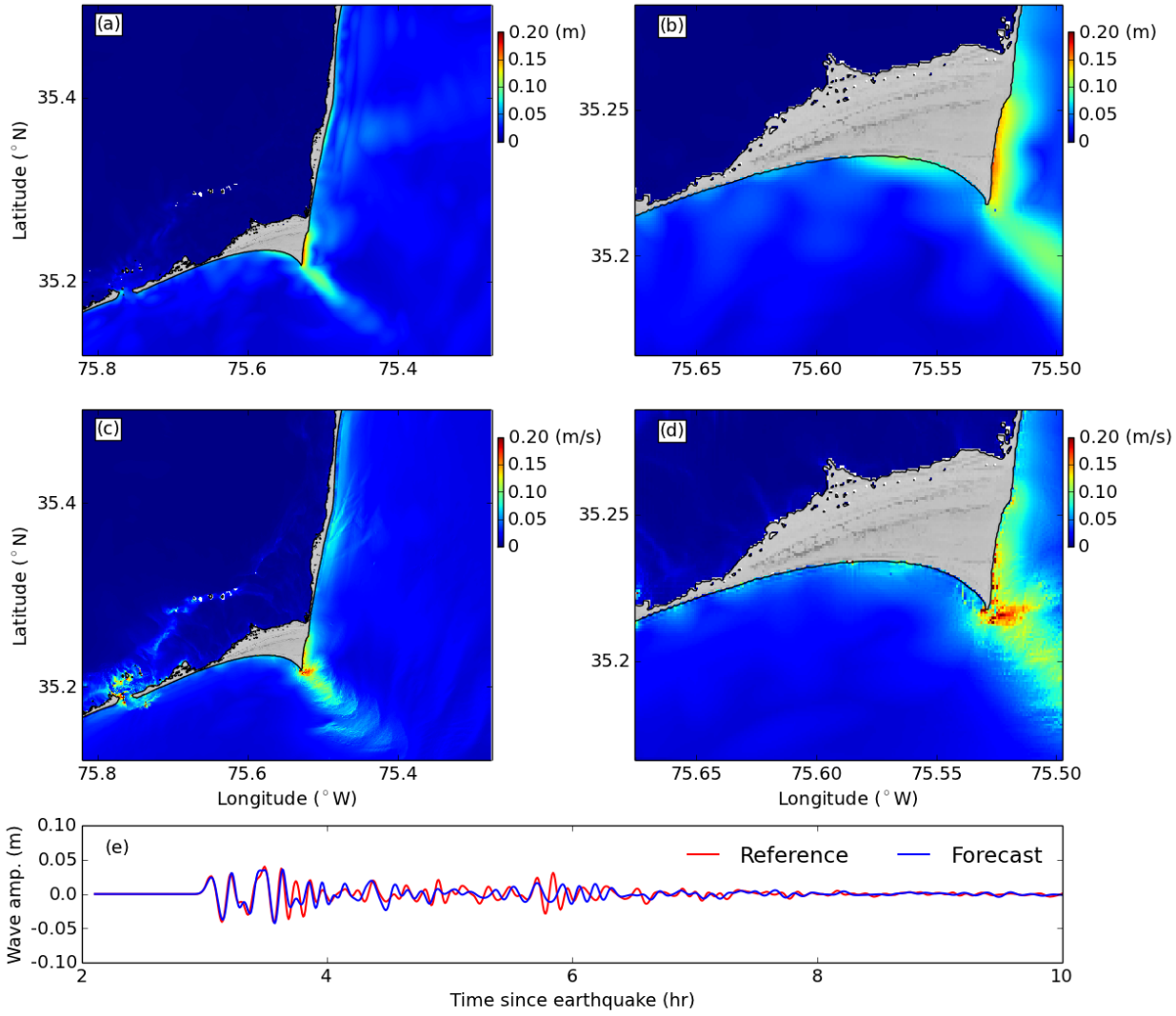

Figure 11: Numerical results for the synthetic scenario of ATSZ B52: maximum water surface elevations near Cape Hatteras, North Carolina, predicted by the reference (a) and forecast models (b), maximum water speeds near Cape Hatteras predicted by the reference (c) and forecast models (d), and time series of wave amplitudes at the warning point (e).

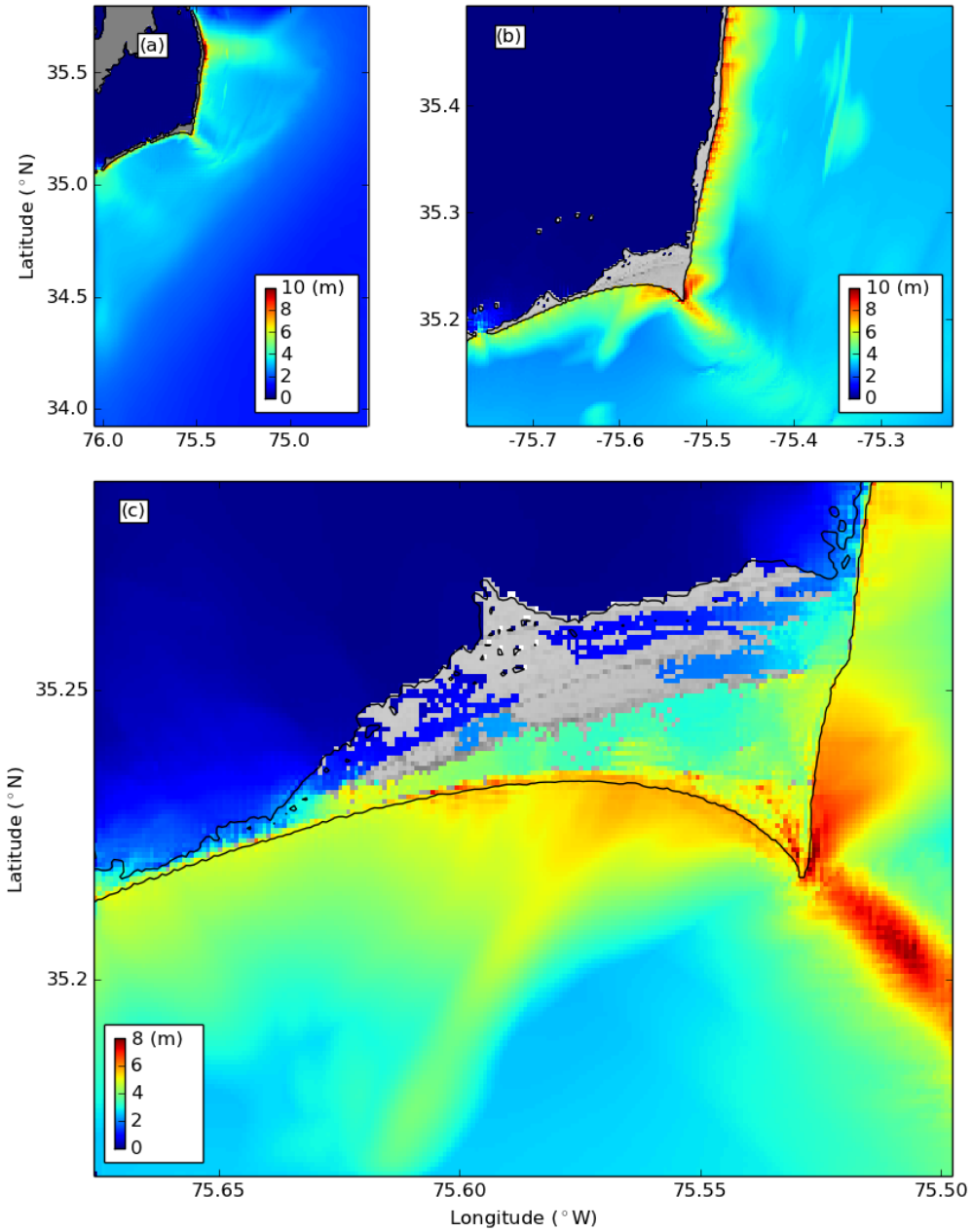

Figure 12: Maximum water surface elevations in the synthetic scenario of ATSZ 48-57 predicted by the forecast model in the A (a), B (b), and C (c) grids.

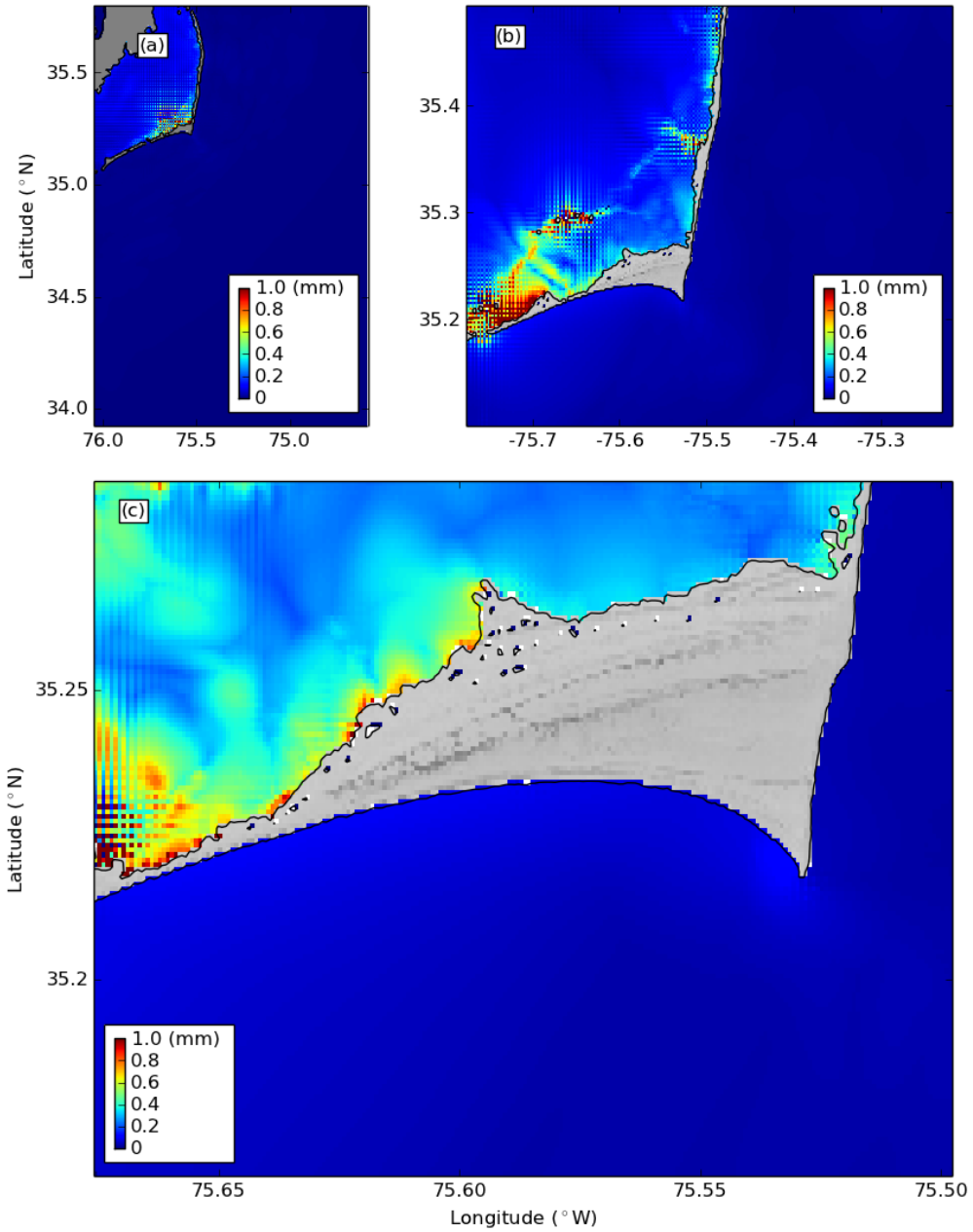

Figure 13: Maximum water surface elevations in the synthetic scenario of SSSZ B11 predicted by the forecast model in the A (a), B (b), and C (c) grids.

Table 1: MOST setup of the reference and forecast models for Cape Hatteras, North Carolina.

		Reference Model				Forecast Model			
Grid	Region	Coverage Lat. (°N) Lon. (°W)	Cell Size	nx×ny	Time Step (sec.)	Coverage Lat. (°N) Lon. (°W)	Cell Size	nx×ny	Time Step (sec.)
A	North Carolina	33.925–35.800 76.050–74.582	12″	441×564	0.85	33.925–35.800 76.050–74.582	24″	211×282	2.55
B	Cape Hatteras	34.896–35.723 75.887–75.117	6″	464×497	0.85	35.100–35.494 75.776–75.219	8″	252×178	2.55
C	Cape Hatteras	35.120–35.502 75.821–75.275	1″	1966×1375	0.85	35.166–35.286 75.676–75.498	3″	215×145	2.55
Minimum offshore depth (m)					0.0				0.0
Water depth for dry land (m)					0.1				0.1
Friction coefficient (n^2)					0.0009				0.0009
CPU time for a 12-hr simulation					$\sim$ 25 hr				$<$ 30 min

Note: All computations are conducted on a 2×6 core @2.93 GHz computer with 12 MB cache in linux 64 RH4 environment.

Table 2: Synthetic tsunami scenarios employed to test the Cape Hatteras, North Carolina, reference and forecast models.

Scenorio No.	Scenario Name	Source Zone	Tsunami Source	α [m]
Mega-tsunami Scenario				
1	ATSZ 38-47	Atlantic	A38-A47, B38-B47	25
2	ATSZ 48-57	Atlantic	A48-A57, B48-B57	25
3	ATSZ 58-67	Atlantic	A58-A67, B58-B67	25
4	ATSZ 68-77	Atlantic	A68-A77, B68-B77	25
5	ATSZ 82-91	Atlantic	A82-A91, B82-B91	25
6	SSSZ 1-10	South Sandwich	A1-A10, B1-B10	25
Mw 7.5 Scenario				
7	ATSZ B52	Atlantic	B52	1
Micro-tsunami Scenario				
8	SSSZ B11	South Sandwich	B11	0.01

A Model *.in files for Cape Hatteras, North Carolina

A.1 Reference model *.in file

0.001	Minimum amp. of input offshore wave (m)
0.0	Minimum depth of offshore (m)
0.1	Dry land depth of inundation (m)
0.0009	Friction coefficient (n**2)
1	run up in a and b
300.0	max wave height meters
0.85	time step (sec)
50825	number of steps for 12 h simulation
1	Compute "A" arrays every n-th time step, n=
1	Compute "B" arrays every n-th time step, n=
36	Input number of steps between snapshots
0	...starting from
1	...saving grid every n-th node, n=

A.2 Forecast model *.in file

0.001	Minimum amp. of input offshore wave (m)
0.0	Minimum depth of offshore (m)
0.1	Dry land depth of inundation (m)
0.0009	Friction coefficient (n**2)
1	run up in a and b
300.0	max wave height meters
2.55	time step (sec)
16941	number of steps for 12 h simulation
1	Compute "A" arrays every n-th time step, n=
1	Compute "B" arrays every n-th time step, n=
12	Input number of steps between snapshots
0	...starting from
1	...saving grid every n-th node, n=

B Propagation Database: Atlantic Ocean Unit Sources

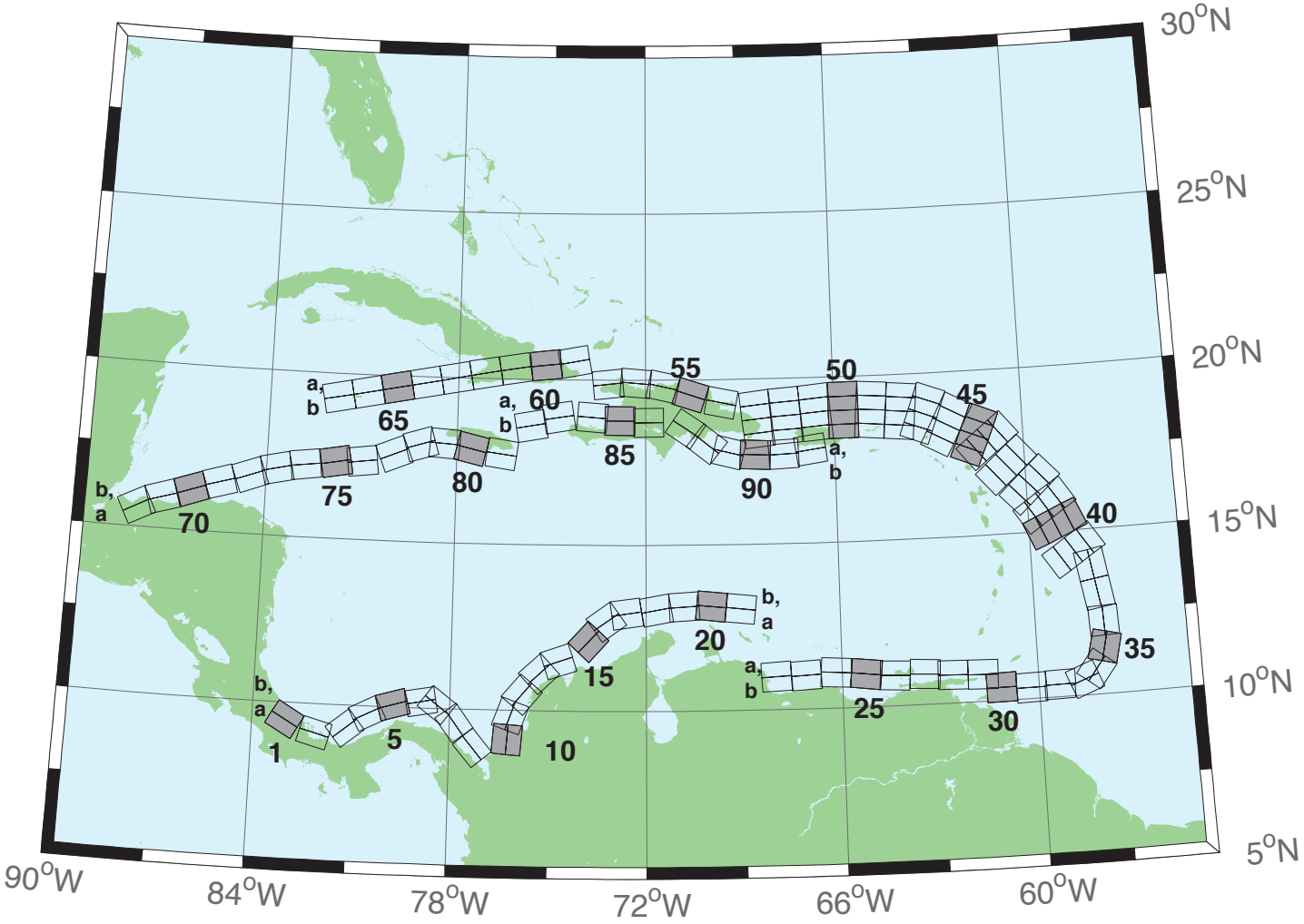

Figure B1: Atlantic Source Zone unit sources.

Table B1: Earthquake parameters for Atlantic Source Zone unit sources.

Segment	Description	Longitude(°E)	Latitude(°N)	Strike(°)	Dip(°)	Depth (km)
atsz–1a	Atlantic Source Zone	-83.2020	9.1449	120	27.5	28.09
atsz–1b	Atlantic Source Zone	-83.0000	9.4899	120	27.5	5
atsz–2a	Atlantic Source Zone	-82.1932	8.7408	105.1	27.5	28.09
atsz–2b	Atlantic Source Zone	-82.0880	9.1254	105.1	27.5	5
atsz–3a	Atlantic Source Zone	-80.9172	9.0103	51.31	30	30
atsz–3b	Atlantic Source Zone	-81.1636	9.3139	51.31	30	5
atsz–4a	Atlantic Source Zone	-80.3265	9.4308	63.49	30	30
atsz–4b	Atlantic Source Zone	-80.5027	9.7789	63.49	30	5
atsz–5a	Atlantic Source Zone	-79.6247	9.6961	74.44	30	30
atsz–5b	Atlantic Source Zone	-79.7307	10.0708	74.44	30	5
atsz–6a	Atlantic Source Zone	-78.8069	9.8083	79.71	30	30
atsz–6b	Atlantic Source Zone	-78.8775	10.1910	79.71	30	5
atsz–7a	Atlantic Source Zone	-78.6237	9.7963	127.2	30	30
atsz–7b	Atlantic Source Zone	-78.3845	10.1059	127.2	30	5
atsz–8a	Atlantic Source Zone	-78.1693	9.3544	143.8	30	30
atsz–8b	Atlantic Source Zone	-77.8511	9.5844	143.8	30	5
atsz–9a	Atlantic Source Zone	-77.5913	8.5989	139.9	30	30
atsz–9b	Atlantic Source Zone	-77.2900	8.8493	139.9	30	5
atsz–10a	Atlantic Source Zone	-75.8109	9.0881	4.67	17	19.62
atsz–10b	Atlantic Source Zone	-76.2445	9.1231	4.67	17	5
atsz–11a	Atlantic Source Zone	-75.7406	9.6929	19.67	17	19.62
atsz–11b	Atlantic Source Zone	-76.1511	9.8375	19.67	17	5
atsz–12a	Atlantic Source Zone	-75.4763	10.2042	40.4	17	19.62
atsz–12b	Atlantic Source Zone	-75.8089	10.4826	40.4	17	5
atsz–13a	Atlantic Source Zone	-74.9914	10.7914	47.17	17	19.62
atsz–13b	Atlantic Source Zone	-75.2890	11.1064	47.17	17	5
atsz–14a	Atlantic Source Zone	-74.5666	11.0708	71.68	17	19.62
atsz–14b	Atlantic Source Zone	-74.7043	11.4786	71.68	17	5
atsz–15a	Atlantic Source Zone	-73.4576	11.8012	42.69	17	19.62
atsz–15b	Atlantic Source Zone	-73.7805	12.0924	42.69	17	5
atsz–16a	Atlantic Source Zone	-72.9788	12.3365	54.75	17	19.62
atsz–16b	Atlantic Source Zone	-73.2329	12.6873	54.75	17	5
atsz–17a	Atlantic Source Zone	-72.5454	12.5061	81.96	17	19.62
atsz–17b	Atlantic Source Zone	-72.6071	12.9314	81.96	17	5
atsz–18a	Atlantic Source Zone	-71.6045	12.6174	79.63	17	19.62
atsz–18b	Atlantic Source Zone	-71.6839	13.0399	79.63	17	5
atsz–19a	Atlantic Source Zone	-70.7970	12.7078	86.32	17	19.62
atsz–19b	Atlantic Source Zone	-70.8253	13.1364	86.32	17	5
atsz–20a	Atlantic Source Zone	-70.0246	12.7185	95.94	17	19.62
atsz–20b	Atlantic Source Zone	-69.9789	13.1457	95.94	17	5
atsz–21a	Atlantic Source Zone	-69.1244	12.6320	95.94	17	19.62
atsz–21b	Atlantic Source Zone	-69.0788	13.0592	95.94	17	5
atsz–22a	Atlantic Source Zone	-68.0338	11.4286	266.9	15	17.94
atsz–22b	Atlantic Source Zone	-68.0102	10.9954	266.9	15	5
atsz–23a	Atlantic Source Zone	-67.1246	11.4487	266.9	15	17.94
atsz–23b	Atlantic Source Zone	-67.1010	11.0155	266.9	15	5
atsz–24a	Atlantic Source Zone	-66.1656	11.5055	273.3	15	17.94
atsz–24b	Atlantic Source Zone	-66.1911	11.0724	273.3	15	5
atsz–25a	Atlantic Source Zone	-65.2126	11.4246	276.4	15	17.94
atsz–25b	Atlantic Source Zone	-65.2616	10.9934	276.4	15	5
atsz–26a	Atlantic Source Zone	-64.3641	11.3516	272.9	15	17.94
atsz–26b	Atlantic Source Zone	-64.3862	10.9183	272.9	15	5
atsz–27a	Atlantic Source Zone	-63.4472	11.3516	272.9	15	17.94
atsz–27b	Atlantic Source Zone	-63.4698	10.9183	272.9	15	5
atsz–28a	Atlantic Source Zone	-62.6104	11.2831	271.1	15	17.94
atsz–28b	Atlantic Source Zone	-62.6189	10.8493	271.1	15	5
atsz–29a	Atlantic Source Zone	-61.6826	11.2518	271.6	15	17.94
atsz–29b	Atlantic Source Zone	-61.6947	10.8181	271.6	15	5
atsz–30a	Atlantic Source Zone	-61.1569	10.8303	269	15	17.94
atsz–30b	Atlantic Source Zone	-61.1493	10.3965	269	15	5
atsz–31a	Atlantic Source Zone	-60.2529	10.7739	269	15	17.94
atsz–31b	Atlantic Source Zone	-60.2453	10.3401	269	15	5
atsz–32a	Atlantic Source Zone	-59.3510	10.8123	269	15	17.94

Continued on next page

Table B1 – continued from previous page

Segment	Description	Longitude(°E)	Latitude(°N)	Strike(°)	Dip(°)	Depth (km)
atsz–32b	Atlantic Source Zone	-59.3734	10.3785	269	15	5
atsz–33a	Atlantic Source Zone	-58.7592	10.8785	248.6	15	17.94
atsz–33b	Atlantic Source Zone	-58.5984	10.4745	248.6	15	5
atsz–34a	Atlantic Source Zone	-58.5699	11.0330	217.2	15	17.94
atsz–34b	Atlantic Source Zone	-58.2179	10.7710	217.2	15	5
atsz–35a	Atlantic Source Zone	-58.3549	11.5300	193.7	15	17.94
atsz–35b	Atlantic Source Zone	-57.9248	11.4274	193.7	15	5
atsz–36a	Atlantic Source Zone	-58.3432	12.1858	177.7	15	17.94
atsz–36b	Atlantic Source Zone	-57.8997	12.2036	177.7	15	5
atsz–37a	Atlantic Source Zone	-58.4490	12.9725	170.7	15	17.94
atsz–37b	Atlantic Source Zone	-58.0095	13.0424	170.7	15	5
atsz–38a	Atlantic Source Zone	-58.6079	13.8503	170.2	15	17.94
atsz–38b	Atlantic Source Zone	-58.1674	13.9240	170.2	15	5
atsz–39a	Atlantic Source Zone	-58.6667	14.3915	146.8	15	17.94
atsz–39b	Atlantic Source Zone	-58.2913	14.6287	146.8	15	5
atsz–39y	Atlantic Source Zone	-59.4168	13.9171	146.8	15	43.82
atsz–39z	Atlantic Source Zone	-59.0415	14.1543	146.8	15	30.88
atsz–40a	Atlantic Source Zone	-59.1899	15.2143	156.2	15	17.94
atsz–40b	Atlantic Source Zone	-58.7781	15.3892	156.2	15	5
atsz–40y	Atlantic Source Zone	-60.0131	14.8646	156.2	15	43.82
atsz–40z	Atlantic Source Zone	-59.6012	15.0395	156.2	15	30.88
atsz–41a	Atlantic Source Zone	-59.4723	15.7987	146.3	15	17.94
atsz–41b	Atlantic Source Zone	-59.0966	16.0392	146.3	15	5
atsz–41y	Atlantic Source Zone	-60.2229	15.3177	146.3	15	43.82
atsz–41z	Atlantic Source Zone	-59.8473	15.5582	146.3	15	30.88
atsz–42a	Atlantic Source Zone	-59.9029	16.4535	137	15	17.94
atsz–42b	Atlantic Source Zone	-59.5716	16.7494	137	15	5
atsz–42y	Atlantic Source Zone	-60.5645	15.8616	137	15	43.82
atsz–42z	Atlantic Source Zone	-60.2334	16.1575	137	15	30.88
atsz–43a	Atlantic Source Zone	-60.5996	17.0903	138.7	15	17.94
atsz–43b	Atlantic Source Zone	-60.2580	17.3766	138.7	15	5
atsz–43y	Atlantic Source Zone	-61.2818	16.5177	138.7	15	43.82
atsz–43z	Atlantic Source Zone	-60.9404	16.8040	138.7	15	30.88
atsz–44a	Atlantic Source Zone	-61.1559	17.8560	141.1	15	17.94
atsz–44b	Atlantic Source Zone	-60.8008	18.1286	141.1	15	5
atsz–44y	Atlantic Source Zone	-61.8651	17.3108	141.1	15	43.82
atsz–44z	Atlantic Source Zone	-61.5102	17.5834	141.1	15	30.88
atsz–45a	Atlantic Source Zone	-61.5491	18.0566	112.8	15	17.94
atsz–45b	Atlantic Source Zone	-61.3716	18.4564	112.8	15	5
atsz–45y	Atlantic Source Zone	-61.9037	17.2569	112.8	15	43.82
atsz–45z	Atlantic Source Zone	-61.7260	17.6567	112.8	15	30.88
atsz–46a	Atlantic Source Zone	-62.4217	18.4149	117.9	15	17.94
atsz–46b	Atlantic Source Zone	-62.2075	18.7985	117.9	15	5
atsz–46y	Atlantic Source Zone	-62.8493	17.6477	117.9	15	43.82
atsz–46z	Atlantic Source Zone	-62.6352	18.0313	117.9	15	30.88
atsz–47a	Atlantic Source Zone	-63.1649	18.7844	110.5	20	22.1
atsz–47b	Atlantic Source Zone	-63.0087	19.1798	110.5	20	5
atsz–47y	Atlantic Source Zone	-63.4770	17.9936	110.5	20	56.3
atsz–47z	Atlantic Source Zone	-63.3205	18.3890	110.5	20	39.2
atsz–48a	Atlantic Source Zone	-63.8800	18.8870	95.37	20	22.1
atsz–48b	Atlantic Source Zone	-63.8382	19.3072	95.37	20	5
atsz–48y	Atlantic Source Zone	-63.9643	18.0465	95.37	20	56.3
atsz–48z	Atlantic Source Zone	-63.9216	18.4667	95.37	20	39.2
atsz–49a	Atlantic Source Zone	-64.8153	18.9650	94.34	20	22.1
atsz–49b	Atlantic Source Zone	-64.7814	19.3859	94.34	20	5
atsz–49y	Atlantic Source Zone	-64.8840	18.1233	94.34	20	56.3
atsz–49z	Atlantic Source Zone	-64.8492	18.5442	94.34	20	39.2
atsz–50a	Atlantic Source Zone	-65.6921	18.9848	89.59	20	22.1
atsz–50b	Atlantic Source Zone	-65.6953	19.4069	89.59	20	5
atsz–50y	Atlantic Source Zone	-65.6874	18.1407	89.59	20	56.3
atsz–50z	Atlantic Source Zone	-65.6887	18.5628	89.59	20	39.2
atsz–51a	Atlantic Source Zone	-66.5742	18.9484	84.98	20	22.1
atsz–51b	Atlantic Source Zone	-66.6133	19.3688	84.98	20	5
atsz–51y	Atlantic Source Zone	-66.4977	18.1076	84.98	20	56.3

Continued on next page

Table B1 – continued from previous page

Segment	Description	Longitude(°E)	Latitude(°N)	Strike(°)	Dip(°)	Depth (km)
atsz–51z	Atlantic Source Zone	-66.5353	18.5280	84.98	20	39.2
atsz–52a	Atlantic Source Zone	-67.5412	18.8738	85.87	20	22.1
atsz–52b	Atlantic Source Zone	-67.5734	19.2948	85.87	20	5
atsz–52y	Atlantic Source Zone	-67.4781	18.0319	85.87	20	56.3
atsz–52z	Atlantic Source Zone	-67.5090	18.4529	85.87	20	39.2
atsz–53a	Atlantic Source Zone	-68.4547	18.7853	83.64	20	22.1
atsz–53b	Atlantic Source Zone	-68.5042	19.2048	83.64	20	5
atsz–53y	Atlantic Source Zone	-68.3575	17.9463	83.64	20	56.3
atsz–53z	Atlantic Source Zone	-68.4055	18.3658	83.64	20	39.2
atsz–54a	Atlantic Source Zone	-69.6740	18.8841	101.5	20	22.1
atsz–54b	Atlantic Source Zone	-69.5846	19.2976	101.5	20	5
atsz–55a	Atlantic Source Zone	-70.7045	19.1376	108.2	20	22.1
atsz–55b	Atlantic Source Zone	-70.5647	19.5386	108.2	20	5
atsz–56a	Atlantic Source Zone	-71.5368	19.3853	102.6	20	22.1
atsz–56b	Atlantic Source Zone	-71.4386	19.7971	102.6	20	5
atsz–57a	Atlantic Source Zone	-72.3535	19.4838	94.2	20	22.1
atsz–57b	Atlantic Source Zone	-72.3206	19.9047	94.2	20	5
atsz–58a	Atlantic Source Zone	-73.1580	19.4498	84.34	20	22.1
atsz–58b	Atlantic Source Zone	-73.2022	19.8698	84.34	20	5
atsz–59a	Atlantic Source Zone	-74.3567	20.9620	259.7	20	22.1
atsz–59b	Atlantic Source Zone	-74.2764	20.5467	259.7	20	5
atsz–60a	Atlantic Source Zone	-75.2386	20.8622	264.2	15	17.94
atsz–60b	Atlantic Source Zone	-75.1917	20.4306	264.2	15	5
atsz–61a	Atlantic Source Zone	-76.2383	20.7425	260.7	15	17.94
atsz–61b	Atlantic Source Zone	-76.1635	20.3144	260.7	15	5
atsz–62a	Atlantic Source Zone	-77.2021	20.5910	259.9	15	17.94
atsz–62b	Atlantic Source Zone	-77.1214	20.1638	259.9	15	5
atsz–63a	Atlantic Source Zone	-78.1540	20.4189	259	15	17.94
atsz–63b	Atlantic Source Zone	-78.0661	19.9930	259	15	5
atsz–64a	Atlantic Source Zone	-79.0959	20.2498	259.2	15	17.94
atsz–64b	Atlantic Source Zone	-79.0098	19.8236	259.2	15	5
atsz–65a	Atlantic Source Zone	-80.0393	20.0773	258.9	15	17.94
atsz–65b	Atlantic Source Zone	-79.9502	19.6516	258.9	15	5
atsz–66a	Atlantic Source Zone	-80.9675	19.8993	258.6	15	17.94
atsz–66b	Atlantic Source Zone	-80.8766	19.4740	258.6	15	5
atsz–67a	Atlantic Source Zone	-81.9065	19.7214	258.5	15	17.94
atsz–67b	Atlantic Source Zone	-81.8149	19.2962	258.5	15	5
atsz–68a	Atlantic Source Zone	-87.8003	15.2509	62.69	15	17.94
atsz–68b	Atlantic Source Zone	-88.0070	15.6364	62.69	15	5
atsz–69a	Atlantic Source Zone	-87.0824	15.5331	72.73	15	17.94
atsz–69b	Atlantic Source Zone	-87.2163	15.9474	72.73	15	5
atsz–70a	Atlantic Source Zone	-86.1622	15.8274	70.64	15	17.94
atsz–70b	Atlantic Source Zone	-86.3120	16.2367	70.64	15	5
atsz–71a	Atlantic Source Zone	-85.3117	16.1052	73.7	15	17.94
atsz–71b	Atlantic Source Zone	-85.4387	16.5216	73.7	15	5
atsz–72a	Atlantic Source Zone	-84.3470	16.3820	69.66	15	17.94
atsz–72b	Atlantic Source Zone	-84.5045	16.7888	69.66	15	5
atsz–73a	Atlantic Source Zone	-83.5657	16.6196	77.36	15	17.94
atsz–73b	Atlantic Source Zone	-83.6650	17.0429	77.36	15	5
atsz–74a	Atlantic Source Zone	-82.7104	16.7695	82.35	15	17.94
atsz–74b	Atlantic Source Zone	-82.7709	17.1995	82.35	15	5
atsz–75a	Atlantic Source Zone	-81.7297	16.9003	79.86	15	17.94
atsz–75b	Atlantic Source Zone	-81.8097	17.3274	79.86	15	5
atsz–76a	Atlantic Source Zone	-80.9196	16.9495	82.95	15	17.94
atsz–76b	Atlantic Source Zone	-80.9754	17.3801	82.95	15	5
atsz–77a	Atlantic Source Zone	-79.8086	17.2357	67.95	15	17.94
atsz–77b	Atlantic Source Zone	-79.9795	17.6378	67.95	15	5
atsz–78a	Atlantic Source Zone	-79.0245	17.5415	73.61	15	17.94
atsz–78b	Atlantic Source Zone	-79.1532	17.9577	73.61	15	5
atsz–79a	Atlantic Source Zone	-78.4122	17.5689	94.07	15	17.94
atsz–79b	Atlantic Source Zone	-78.3798	18.0017	94.07	15	5
atsz–80a	Atlantic Source Zone	-77.6403	17.4391	103.3	15	17.94
atsz–80b	Atlantic Source Zone	-77.5352	17.8613	103.3	15	5
atsz–81a	Atlantic Source Zone	-76.6376	17.2984	98.21	15	17.94

Continued on next page

Table B1 – continued from previous page

Segment	Description	Longitude(°E)	Latitude(°N)	Strike(°)	Dip(°)	Depth (km)
atsz–81b	Atlantic Source Zone	-76.5726	17.7278	98.21	15	5
atsz–82a	Atlantic Source Zone	-75.7299	19.0217	260.1	15	17.94
atsz–82b	Atlantic Source Zone	-75.6516	18.5942	260.1	15	5
atsz–83a	Atlantic Source Zone	-74.8351	19.2911	260.8	15	17.94
atsz–83b	Atlantic Source Zone	-74.7621	18.8628	260.8	15	5
atsz–84a	Atlantic Source Zone	-73.6639	19.2991	274.8	15	17.94
atsz–84b	Atlantic Source Zone	-73.7026	18.8668	274.8	15	5
atsz–85a	Atlantic Source Zone	-72.8198	19.2019	270.6	15	17.94
atsz–85b	Atlantic Source Zone	-72.8246	18.7681	270.6	15	5
atsz–86a	Atlantic Source Zone	-71.9143	19.1477	269.1	15	17.94
atsz–86b	Atlantic Source Zone	-71.9068	18.7139	269.1	15	5
atsz–87a	Atlantic Source Zone	-70.4738	18.8821	304.5	15	17.94
atsz–87b	Atlantic Source Zone	-70.7329	18.5245	304.5	15	5
atsz–88a	Atlantic Source Zone	-69.7710	18.3902	308.9	15	17.94
atsz–88b	Atlantic Source Zone	-70.0547	18.0504	308.4	15	5
atsz–89a	Atlantic Source Zone	-69.2635	18.2099	283.9	15	17.94
atsz–89b	Atlantic Source Zone	-69.3728	17.7887	283.9	15	5
atsz–90a	Atlantic Source Zone	-68.5059	18.1443	272.9	15	17.94
atsz–90b	Atlantic Source Zone	-68.5284	17.7110	272.9	15	5
atsz–91a	Atlantic Source Zone	-67.6428	18.1438	267.8	15	17.94
atsz–91b	Atlantic Source Zone	-67.6256	17.7103	267.8	15	5
atsz–92a	Atlantic Source Zone	-66.8261	18.2536	262	15	17.94
atsz–92b	Atlantic Source Zone	-66.7627	17.8240	262	15	5

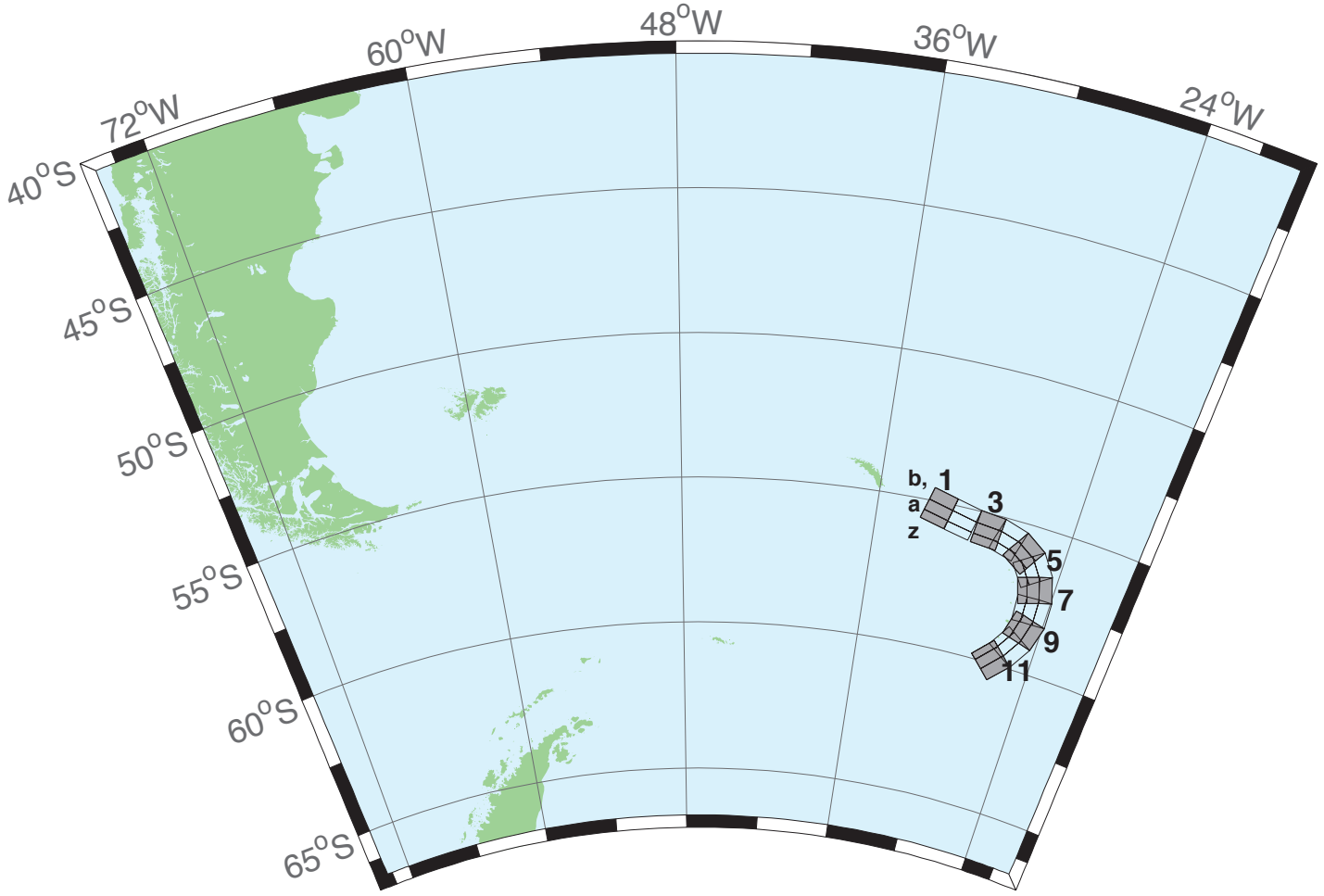

Figure B2: South Sandwich Islands Subduction Zone.

Table B2: Earthquake parameters for South Sandwich Islands Subduction Zone unit sources.

Segment	Description	Longitude(°E)	Latitude(°N)	Strike(°)	Dip(°)	Depth (km)
sssz–1a	South Sandwich Islands Subduction Zone	-32.3713	-55.4655	104.7	28.53	17.51
sssz–1b	South Sandwich Islands Subduction Zone	-32.1953	-55.0832	104.7	9.957	8.866
sssz–1z	South Sandwich Islands Subduction Zone	-32.5091	-55.7624	104.7	46.99	41.39
sssz–2a	South Sandwich Islands Subduction Zone	-30.8028	-55.6842	102.4	28.53	17.51
sssz–2b	South Sandwich Islands Subduction Zone	-30.6524	-55.2982	102.4	9.957	8.866
sssz–2z	South Sandwich Islands Subduction Zone	-30.9206	-55.9839	102.4	46.99	41.39
sssz–3a	South Sandwich Islands Subduction Zone	-29.0824	-55.8403	95.53	28.53	17.51
sssz–3b	South Sandwich Islands Subduction Zone	-29.0149	-55.4468	95.53	9.957	8.866
sssz–3z	South Sandwich Islands Subduction Zone	-29.1353	-56.1458	95.53	46.99	41.39
sssz–4a	South Sandwich Islands Subduction Zone	-27.8128	-55.9796	106.1	28.53	17.51
sssz–4b	South Sandwich Islands Subduction Zone	-27.6174	-55.5999	106.1	9.957	8.866
sssz–4z	South Sandwich Islands Subduction Zone	-27.9659	-56.2744	106.1	46.99	41.39
sssz–5a	South Sandwich Islands Subduction Zone	-26.7928	-56.2481	123.1	28.53	17.51
sssz–5b	South Sandwich Islands Subduction Zone	-26.4059	-55.9170	123.1	9.957	8.866
sssz–5z	South Sandwich Islands Subduction Zone	-27.0955	-56.5052	123.1	46.99	41.39
sssz–6a	South Sandwich Islands Subduction Zone	-26.1317	-56.6466	145.6	23.28	16.11
sssz–6b	South Sandwich Islands Subduction Zone	-25.5131	-56.4133	145.6	9.09	8.228
sssz–6z	South Sandwich Islands Subduction Zone	-26.5920	-56.8194	145.6	47.15	35.87
sssz–7a	South Sandwich Islands Subduction Zone	-25.6787	-57.2162	162.9	21.21	14.23
sssz–7b	South Sandwich Islands Subduction Zone	-24.9394	-57.0932	162.9	7.596	7.626
sssz–7z	South Sandwich Islands Subduction Zone	-26.2493	-57.3109	162.9	44.16	32.32
sssz–8a	South Sandwich Islands Subduction Zone	-25.5161	-57.8712	178.2	20.33	15.91
sssz–8b	South Sandwich Islands Subduction Zone	-24.7233	-57.8580	178.2	8.449	8.562
sssz–8z	South Sandwich Islands Subduction Zone	-26.1280	-57.8813	178.2	43.65	33.28
sssz–9a	South Sandwich Islands Subduction Zone	-25.6657	-58.5053	195.4	25.76	15.71
sssz–9b	South Sandwich Islands Subduction Zone	-24.9168	-58.6127	195.4	8.254	8.537
sssz–9z	South Sandwich Islands Subduction Zone	-26.1799	-58.4313	195.4	51.69	37.44
sssz–10a	South Sandwich Islands Subduction Zone	-26.1563	-59.1048	212.5	32.82	15.65
sssz–10b	South Sandwich Islands Subduction Zone	-25.5335	-59.3080	212.5	10.45	6.581
sssz–10z	South Sandwich Islands Subduction Zone	-26.5817	-58.9653	212.5	54.77	42.75
sssz–11a	South Sandwich Islands Subduction Zone	-27.0794	-59.6799	224.2	33.67	15.75
sssz–11b	South Sandwich Islands Subduction Zone	-26.5460	-59.9412	224.2	11.32	5.927
sssz–11z	South Sandwich Islands Subduction Zone	-27.4245	-59.5098	224.2	57.19	43.46

C Forecast Model Testing

Author: Lindsey Wright

C.1 Purpose

Forecast models are tested with synthetic tsunami events covering a range of tsunami source locations and magnitudes. Testing is also done with selected historical tsunami events when available.

The purpose of forecast model testing is three-fold. The first objective is to assure that the results obtained with the NOAAs tsunami forecast system software, which has been released to the Tsunami Warning Centers for operational use, are consistent with those obtained by the researcher during the development of the forecast model. The second objective is to test the forecast model for consistency, accuracy, time efficiency, and quality of results over a range of possible tsunami locations and magnitudes. The third objective is to identify bugs and issues in need of resolution by the researcher who developed the forecast model or by the forecast software development team before the next version release to NOAA's two Tsunami Warning Centers.

Local hardware and software applications, and tools familiar to the researcher(s), are used to run MOST model during the forecast model development. The test results presented in this report lend confidence that the model performs as developed and produces the same results when initiated within the forecast system application in an operational setting as those produced by the researcher during the forecast model development. The test results assure those who rely on the Cape Hatteras tsunami forecast model that consistent results are produced irrespective of system.

C.2 Testing procedure

The general procedure for forecast model testing is to run a set of synthetic tsunami scenarios through the forecast system application and compare the results with those obtained by the researcher during the forecast model development and presented in the Tsunami Forecast Model Report. Specific steps taken to test the model include:

1. Identification of testing scenarios, including the standard set of synthetic events and customized synthetic scenarios that may have been used by the researcher(s) in developing the forecast model.

2. Creation of new events to represent customized synthetic scenarios used by the researcher(s) in developing the forecast model, if any.

3. Submission of test model runs with the forecast system, and export of the results from A, B, and C grids, along with time series.

4. Recording applicable metadata, including the specific version of the forecast system used for testing.

5. Examination of forecast model results from the forecast system for instabilities in both time series and plot results.

6. Comparison of forecast model results obtained through the forecast system with those obtained during the forecast model development.

7. Summarization of results with specific mention of quality, consistency, and time efficiency.

8. Reporting of issues identified to modeler and forecast software development team.

9. Retesting the forecast models in the forecast system when reported issues have been addressed or explained.

Synthetic model runs were tested on a DELL PowerEdge R510 computer equipped with two Xeon E5670 processors at 2.93 Ghz, each with 12 MBytes of cache and 32 GB memory. The processors are hex core and support hyper threading, resulting in the computer performing as a 24 processor core machine. Additionally, the testing computer supports 10 Gigabit Ethernet for fast network connections. This computer configuration is similar or the same as the configurations of the computers installed at the Tsunami Warning Centers so the compute times should only vary slightly.

C.3 Results

The Cape Hatteras forecast model was tested with SIFT version 3.2 for three synthetic scenarios. Test results from the forecast system and comparisons with the results obtained during the forecast model development are shown numerically in Table C1 and graphically in Figures C1 to C3. The results show that the minimum and maximum amplitudes and time series obtained from the forecast system agree with those obtained during the forecast model development, and that the forecast model is stable and robust, with consistent and high-quality results across geographically distributed tsunami sources. The model run time (wall-clock time) was 16.45 min for 12 hr of simulation time, and 5.48 min for 4.0 hr. This is within the 10 min run time for 4 hr of simulation and satisfies run time requirements.

A suite of three synthetic events was run on the Cape Hatteras forecast model. The modeled scenarios were stable for all cases run with no inconsistencies or ringing. The largest modeled height was 467.9 centimeters (cm) from the Atlantic (ATSZ 48-57) source zone. The smallest signal of 40.7 cm was recorded at the far field South Sandwich (SSSZ 1-10) source zone. Comparisons between the development cases and the forecast system output were consistent in shape and amplitude for all cases run. The Cape Hatteras reference point used for the forecast model development is the same as what is deployed in the forecast system, so the results can be considered valid for the three cases studied.

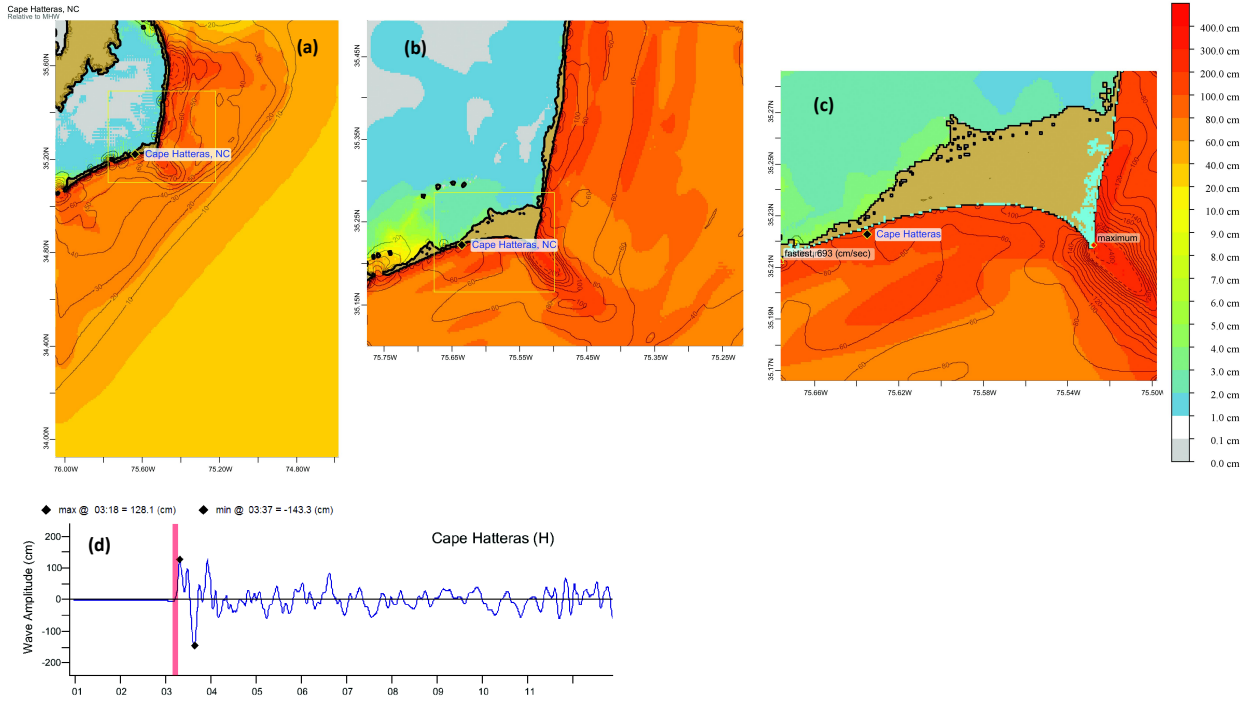

Figure C1: Response of the Cape Hatteras forecast model to synthetic scenario ATSZ 38-47 (alpha=25). Maximum sea surface elevation for (a) A grid, (b) B grid, and (c) C grid. Sea surface elevation time series at the C-grid warning point (d).

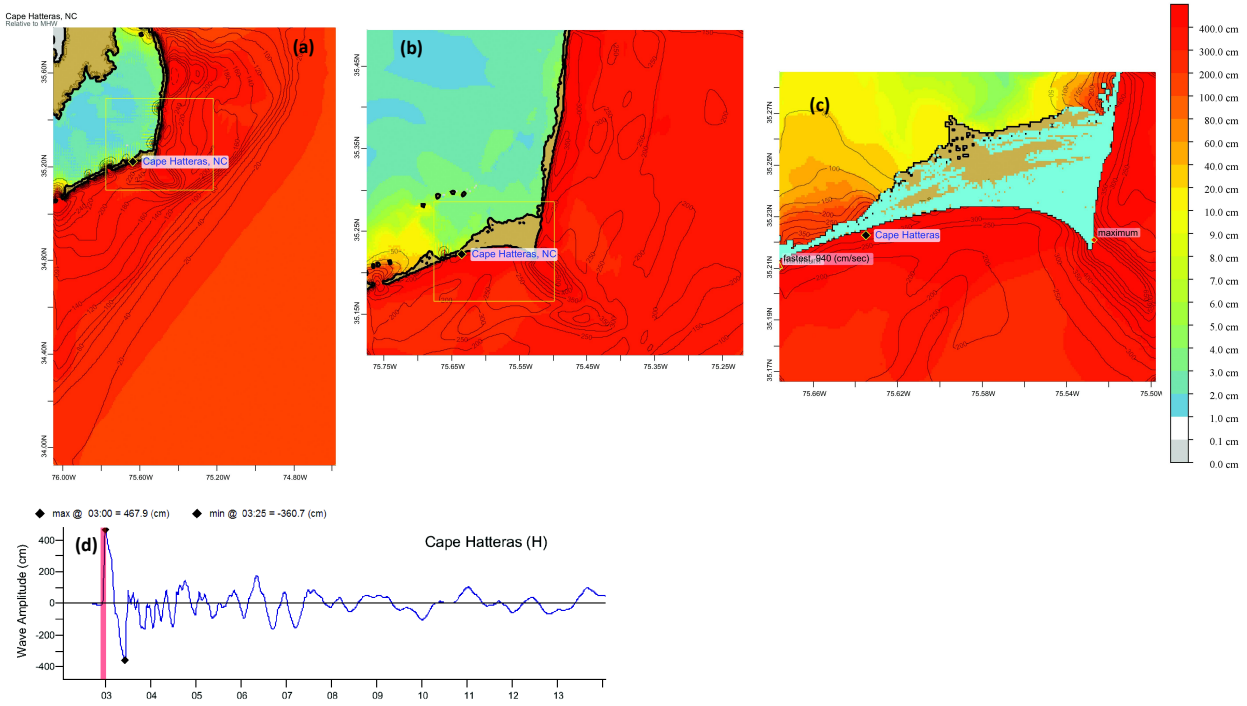

Figure C2: Response of the Cape Hatteras forecast model to synthetic scenario ATSZ 48-57 (alpha=25). Maximum sea surface elevation for (a) A grid, (b) B grid, and (c) C-grid. Sea surface elevation time series at the C-grid warning point (d).

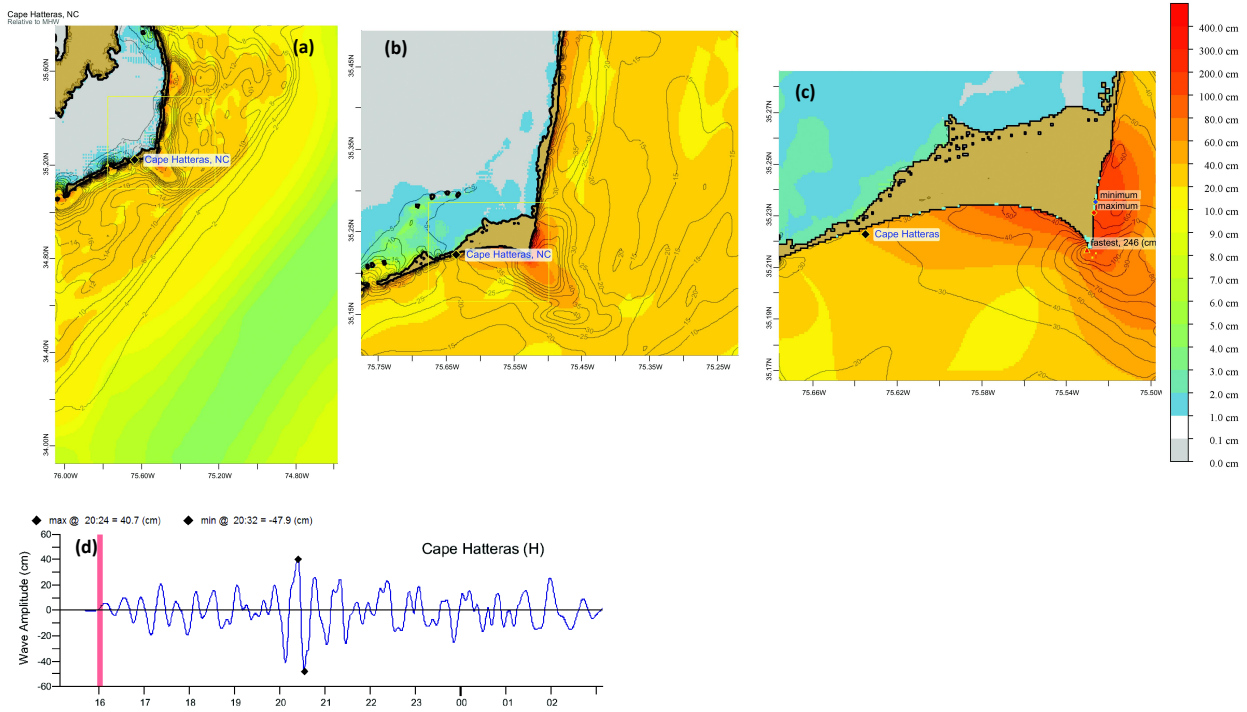

Figure C3: Response of the Morehead City forecast model to synthetic scenario SSSZ 1-10 (alpha=25). Maximum sea surface elevation for (a) A grid, (b) B grid, and (c) C grid. Sea surface elevation time series at the C-grid warning point (d).

Table C1: Table of maximum and minimum amplitudes (cm) at the Cape Hatteras warning point for synthetic and historical events tested using SIFT 3.2 and obtained during development.

Scenario Name	**Source Zone**	**Tsunami Source**	α **[m]**	**SIFT Max (cm)**	**Development Max (cm)**	**SIFT Min (cm)**	**Development Min (cm)**
Mega-tsunami Scenarios							
ATSZ 38-47	Atlantic	A38-A47, B38-B47	25	128.1	128.1	-143.3	-144.3
ATSZ 48-57	Atlantic	A34-A57, B48-B57	25	467.9	467.8	-360.7	-360.6
SSSZ 1-10	South Sandwich Islands	A1-A10, B1-B10	25	40.7	40.7	-47.9	-48.0